



TEXT AND REFERENCES ACCOMPANYING NEVADA BUREAU OF MINES AND GEOLOGY OPEN-FILE REPORT 2023-11

# Geologic Map of Rhyolite Ridge and the Northern Silver Peak Range, Esmeralda County, Nevada

by

Izabella Ogilvie<sup>1</sup>, Michael H. Darin<sup>1,2</sup>, John T. Reynolds<sup>3</sup>,  
Daniel A. Chafetz<sup>1,3</sup>, and Matthieu Harlaux<sup>1,4</sup>

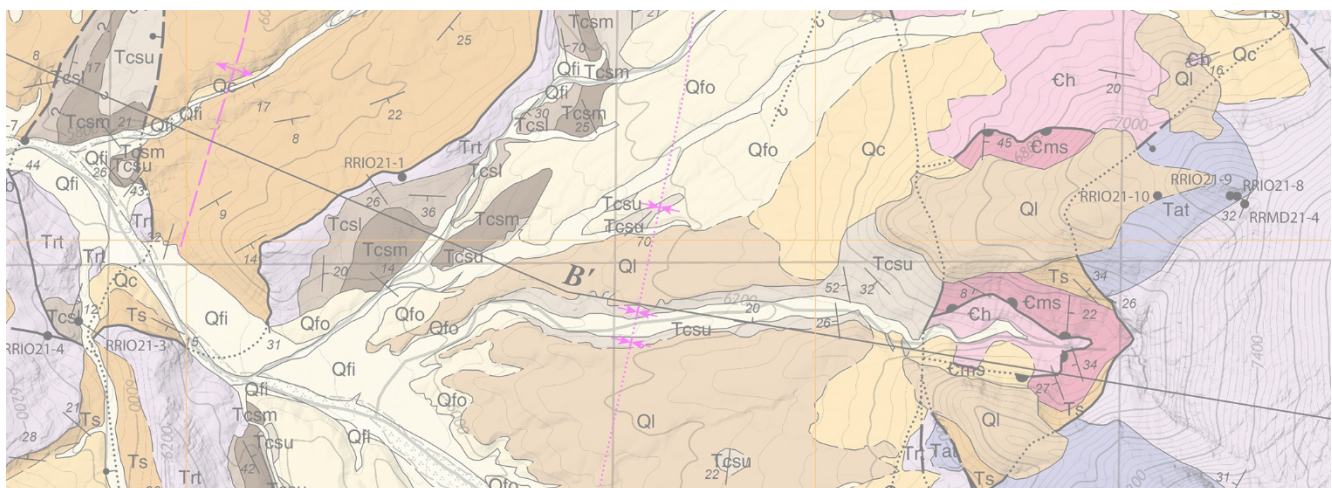
<sup>1</sup> Nevada Bureau of Mines and Geology, University of Nevada, Reno

<sup>2</sup> Oregon Department of Geology and Mineral Industries, Portland, OR

<sup>3</sup> Ioneer USA Corporation, Reno, NV

<sup>4</sup> Bureau de Recherches Géologiques et Minières, Orléans, France

2023



© Copyright 2023 The University of Nevada, Reno. All Rights Reserved.

**Suggested citation:**

Ogilvie, I., Darin, M.H., Reynolds, J.T., Chafetz, D.A., and Harlaux, M., 2023, Geologic map of Rhyolite Ridge and the northern Silver Peak Range, Esmeralda County, Nevada: Nevada Bureau of Mines and Geology Open-File Report 2023-11, scale 1:24,000, 35 p.

*NBNG open-file reports have not undergone formal peer review. This geologic map was funded in part by the USGS National Cooperative Geologic Mapping Program under Earth Mapping Resources Initiative (Earth MRI) award number G21AC10365, 2021.*

## ABSTRACT

Rhyolite Ridge is located in the northern Silver Peak Range of southwestern Nevada and contains significant sediment-hosted lithium and boron deposits that are nearing development. Despite the economic importance of these resources, the primary source of lithium, deformation history, and the relative influences of structural, stratigraphic, and magmatic controls on lithium enrichment are uncertain. This report presents new 1:24,000-scale geologic mapping, whole-rock geochemistry, and a sub-regional compilation of Cenozoic geochronologic data to support the evaluation and assessment of these critical minerals through the U.S. Geological Survey (USGS) Earth Mapping Resources Initiative (Earth MRI). Most of the economic lithium and boron mineralization occurs in the upper Miocene to lower Pliocene Cave Spring formation, which is composed of interbedded lacustrine claystone, marl, limestone, volcaniclastic rocks, and tuffs. Anomalously high concentrations of lithium (up to 2,620 ppm; Reynolds and Chafetz, 2020) are bound in marl, smectite, and mixed illite-smectite clays, while boron is primarily associated with searlesite. The Cave Spring formation is mostly contained within a single structural basin in the study area and was deposited in an alluvial-lacustrine environment on top of ~6.1–5.8 Ma rhyolitic tuffs and lavas of the Rhyolite Ridge and Argentite Canyon formations. Geochemical data from these pre-basin volcanic rocks contain exceptionally high whole-rock lithium concentrations up to 451 ppm, though with notable spatial heterogeneity. The high lithium (and boron) concentrations and considerable spatial extent and volume of these rhyolites implicate them as a probable source for the mineralization in the Cave Spring formation. The White Hill and Cave Spring faults are a pair of conjugate normal faults that controlled deposition of the Cave Spring formation in an internally drained, alluvial-lacustrine basin that experienced WNW-directed extension since latest Miocene time (Ogilvie, 2023). Field relations, subsurface well data, airborne electromagnetic surveys, and our synthesis of geochronologic constraints indicate a similar style of extension across the study area associated with both NW- and SE-dipping normal faults. Active faulting and basin subsidence continues today near the western map boundary along the Emigrant Peak fault zone that bounds northern Fish Lake Valley.

## INTRODUCTION

The Rhyolite Ridge area in southwestern Nevada is situated in one of the richest lithium districts in the state and the nation. Located within the northern Silver Peak Range and adjacent to one of North America's only producing lithium brine operations in Clayton Valley (Albemarle), Rhyolite Ridge contains economically important sediment-hosted lithium and boron deposits that are nearing development. Lithium and boron mineralization occurs as stratiform lake deposits within the upper Miocene to Pliocene Cave Spring formation of Oldow et al. (2009). Despite their importance, the specific factors and processes that are most critical in generating sediment-hosted lithium resources and lithium-rich brine systems are not well understood. The area is partly covered by existing small- to moderate-scale (1:250,000 to 1:62,500) geologic maps (Albers and Stewart, 1972; Stewart et al., 1974; Robinson et al., 1976); however, detailed mapping of the lithium- and boron-enriched sedimentary rocks and their relations with interbedded volcanic units and structures are lacking (fig. 1). Hence, Rhyolite Ridge and greater Clayton Valley were recently identified as a strategic focus area for the USGS-funded Earth Mapping Resources Initiative, or Earth MRI. This program seeks to identify potential critical mineral resources, like lithium, and to improve our understanding of the geologic framework associated with their development through new detailed geologic mapping and geophysical data acquisitions. The primary goals of Earth MRI are to enhance U.S. domestic supplies of critical minerals and to minimize reliance on foreign sources of minerals that are fundamental to our national security and economy.

This report presents new detailed geologic mapping, a compilation of geochronologic data from the greater Clayton Valley focus area (table 1), and new whole-rock geochemical data from the Rhyolite Ridge study area (table 2). Geologic mapping has been greatly enhanced by the incorporation of newly acquired lidar topographic and airborne electromagnetic datasets provided by the USGS and DOE Geoscience Data Acquisition for Western Nevada (GeoDAWN) project, a joint effort between the USGS and the U.S. Department of Energy (DOE). These remote sensing datasets were instrumental in supplementing reconnaissance mapping and field studies in areas along the map boundaries and enhancing detailed mapping and the construction of structural cross sections within the core study area (fig. 2).

## TECTONIC SETTING

Clayton Valley is located in Esmeralda County, Nevada, approximately 160 kilometers (100 miles) north of Death Valley, CA, and approximately halfway between the cities of Reno and Las Vegas, NV. The valley is surrounded by fault-bounded ranges on all sides that include the Silver Peak Range to the west, Clayton Ridge and the Montezuma Range to the east, the Palmetto Mountains and Silver Peak Range to the south, and Big Smoky Valley, Paymaster Ridge, and the Weepah Hills to the north (fig. 1). The Rhyolite Ridge study area is located within the southern Walker Lane fault system, a zone of active dextral transtension in western Nevada that accommodates ~20% (10–11 mm yr<sup>-1</sup>) of cumulative Pacific-North American plate motion (Dokka and Travis, 1990; Bennett et al., 2003; Faulds and Henry, 2008; Lifton et al., 2013). The greater Clayton Valley area lies directly south of the Mina deflection, a complex zone of ENE-striking left-lateral faults that represents a major right step in the Walker Lane belt that transfers strain from the NW-striking dextral Fish Lake Valley–Death Valley fault zone to various NW-striking dextral faults of the central Walker Lane belt (Faulds and Henry, 2008). Active faulting is well documented from geodetic and paleoseismic studies in the region (Reheis and Sawyer, 1997; Angster et al., 2019) and was vividly expressed during the recent M6.5 Monte Cristo Range earthquake on May 15, 2020, which occurred ~28 km north of the study area and represents the largest recorded seismic event in Nevada in the past 66 years (Hammond et al., 2020; Koehler et al., 2021).

## DESCRIPTION OF MAP UNITS

### Quaternary Deposits

**Qfy Young alluvium and alluvial-fan deposits (Holocene)** Locally derived, unconsolidated, coarse-grained alluvial deposits in intermittently active alluvial fans and washes; typically composed of sandy pebble- to cobble-sized gravel with boulders. At range fronts and adjacent to steep bedrock outcrops, Qfy grades into and includes young pediment veneers of colluvium. Clasts are subrounded to subangular and generally poorly sorted. Surfaces have complex distributary flow patterns with morphology ranging from fresh bar-and-channel forms to slightly smoothed surfaces with moderately developed gravel pavement and light rock varnish on volcanic clasts. Includes abandoned terraces 0.25–2 m above active washes. Typically has weak to no soil development. If present, soil development is characterized by Stage I CaCO<sub>3</sub> coatings on bottoms of clasts. Exposed thickness is usually less than 3 m.

**Qc Colluvium (Holocene to early Pleistocene)** Angular to slightly rounded, poorly sorted boulders to pebbles in a variably sandy matrix. Locally derived and confined to rockfall-prone slopes or present at the bases of steep bedrock slopes. Colluvium deposits generally grade into, and are commonly included within, alluvial-fan map units. Where colluvium is identified, it is undivided by age and includes very young unconsolidated deposits through semi-consolidated abandoned surfaces. Soil development varies from minimal to stage II CaCO<sub>3</sub> Bk horizons. Thickness is less than 5 m.

**Ql Landslide deposits (Holocene to Pleistocene)** Angular to subangular, mostly unconsolidated and unsorted boulders to pebbles in a variable clayey to sandy matrix. Outsized blocks are up to 5–7 m in diameter. Typically composed of a conspicuously monolithologic assemblage of volcanic clasts. These deposits are commonly located adjacent to steep topography and/or downslope of gently to moderately volcanic strata that form bedrock dip-slopes. Individual landslide deposits reach up to ~60 m thick near range fronts and thin gradually away from high topography to more typical thicknesses of 2–10 m.

**Qfi Intermediate-aged alluvial-fan deposits (early Holocene to middle Pleistocene)** Coarse-grained alluvial deposits in mostly inactive alluvial fans and terraces; typically sandy pebble- to cobble-sized gravel with boulders. At range fronts, Qfi commonly includes abandoned, moderately cemented pediment veneers of colluvium. Clasts are subrounded to subangular and poorly sorted. Surface morphology is planar with moderately developed gravel pavement and weak to dark varnish on volcanic clasts, and Stage I–III CaCO<sub>3</sub> horizons up 1 m thick. Incised drainages have a tributary pattern with channel incision typically less than 5 m. Exposed thickness of this unit rarely exceeds 10 m.

**Qfo Older alluvial-fan deposits (middle to early Pleistocene)** Coarse-grained alluvial deposits on inactive or relict alluvial fans and terraces; typically sandy pebble- to cobble-sized gravel with boulders. At range fronts, Qfo commonly includes abandoned, moderately cemented pediment veneers of colluvium. Generally poorly sorted with subrounded to subangular clasts, and weakly consolidated to well cemented by caliche. Surface morphology varies from planar and smooth with erosionally rounded margins to fully rounded erosional remnants. Planar surfaces commonly display tightly packed gravel pavement, dark to very dark varnish, and some surface litter of pedogenic carbonate clasts. Upper soil horizons are erosionally stripped, Stage III–IV CaCO<sub>3</sub> horizons up to 2 m

thick. Broader surfaces are highly dissected by tributary channels up to 10 m deep. Thickness typically ranges from 1–15 m.

## Neogene Sedimentary Rocks

### *Fish Lake Valley assemblage (middle Pleistocene to early Pliocene)*

The Fish Lake Valley assemblage was informally named by Oldow et al. (2009) for the heterolithic sequence of poorly lithified claystone, siltstone, sandstone, and interbedded basaltic lavas in the northwestern part of the Silver Peak Range and study area. This unit corresponds to “Sedimentary Unit 6” of Robinson et al. (1976). Here we include units Tf and QTf (“QTg” of Robinson et al., 1976) as informal lower and upper members, respectively, of the Fish Lake Valley assemblage, which is dated at ~3.76 to <0.76 Ma based on dating and correlation of interbedded lavas and tuffs (Reheis and Sawyer, 1997; Oldow et al., 2009).

**QTf Conglomerates with minor sandstones and oldest alluvial-fan deposits** Coarse-grained, high-standing alluvial deposits in relict alluvial fans abandoned by deep dissection. Mostly composed of interbedded sandy gravel and sand that is weakly consolidated and well to moderately stratified and sorted. Locally contains lenses or thin beds of tuffaceous sandstone and volcanic ash to lapilli tuffs. Fine-grained lacustrine facies are less common. Grain size is chiefly comprised of cobble- and boulder-gravels with subangular to subrounded clasts. Clast composition varies from being dominated by volcanic lithologies in the south to Paleozoic basement lithologies like chert, carbonate, and quartzite in the north. Tephrochronology studies of multiple tuffs in QTf suggest they correlate with various regional 2.8–0.76 Ma tephras including the tuffs of Taylor Canyon and the Bishop Tuff (Reheis, 1991; Reheis and Sawyer, 1997). These gravels were likely derived from alluvial fans emanating from the northern Silver Peak Range. The total thickness of QTf is at least 350 m and may reach a maximum of 1000 m just west of the Emigrant Peak fault zone in northern Fish Lake Valley based on subsurface data (Reheis and Sawyer, 1997).

**Tf Fluvial and lacustrine sandstones, mudstones, and conglomerates** Mostly white, pale yellow, and greenish-gray, thin- to medium-bedded and well-stratified pebbly sandstone, tuffaceous sandstone, mudstone, conglomerate, and tuffs. Sandstones are generally poorly to moderately sorted, evenly bedded,

with subplanar bedding planes that locally show pinch-and-swell and channel scour geometries. Wavy bedding and ripple cross-stratification are subtle but common. Volcanic lithic fragments and biotite are common as in sandier facies. Conglomerates are well cemented, normally graded, and usually occur as lenticular channels. Clasts are dominated by pale green to pink rhyolite tuff (Trt), dark maroon aphanitic rhyolite (Trlb), and tan mudstone rip ups in the south, and Paleozoic chert, limestone, and quartzite in the north. Though poorly exposed, mudstones are typically clay-rich and diagnostically green to grayish-orange. Claystone facies commonly contain ulexite, a white, fibrous borate that locally forms conspicuously reworked cm-scale clasts or efflorescences on some erosional surfaces. Basalt flows near the base of the Fish Lake Valley assemblage in the southwest part of the map area yield whole-rock  $^{40}\text{Ar}/^{39}\text{Ar}$  dates of  $3.76 \pm 0.04$  and  $3.71 \pm 0.01$  Ma (Oldow et al., 2009). Thickness varies up to ~550 m.

### *Cave Spring formation (early Pliocene to latest Miocene)*

Interbedded lacustrine claystone, marl, limestone, volcanics and tuffs containing anomalously high concentrations of lithium and boron bound in marl-illite-smectite clays and the sodium borosilicate searlesite, respectively (Reynolds and Chafetz, 2020; Chafetz, 2023). Distinctive, normally graded, lithic- and pumice-rich tuffs or ‘gritstones’ interrupt the sequence and delineate lower, middle, and upper members, as described in detail below. The Cave Spring formation was previously referred to as “Sedimentary Unit 4” by Robinson et al. (1976) and described as a local unit of Miocene or Pliocene age composed of sandstone and siltstone with minor limestone near its base. Oldow et al. (2009) informally assigned it the name “Cave Springs Formation” and described the unit as being composed of detritus derived from the tuff of Rhyolite Ridge (Trt) and older Paleozoic units. Reynolds and Chafetz (2020) provide a detailed analysis of sedimentology, stratigraphy, and anomalously high concentrations of lithium and boron within this unit. They also propose a revision to the name of this unit as the singular “Cave Spring formation” based on the name of “Cave Spring” derived from existing USGS topographic maps. Here we abandon the former “Cave Springs Formation” and follow Reynolds and Chafetz (2020) in adopting the informal name “Cave Spring formation” for this unit, and we recommend its continued use in future studies.

**Tcsu Upper member** Gray, uniform, thinly bedded siltstone and lesser fine-grained sandstone and gritstones. This informally named member corresponds with the G4 and S3 sub-units of the Cave Spring formation defined by Reynolds and Chafetz (2020). The base of Tcsu consists of 8–10 m of resistant gritstone that is dark gray where fresh but weathers beige to rusty orange due to oxidation (G4). This is in turn overlain by up to ~240 m of reduced, drab, siltstone with numerous thin, intercalated, white to greenish-gray tuffs and gritstones (S3). Northeast of Beacon Hill, the Cave Spring formation consists of coarse, unsorted cobble-boulder conglomerates composed exclusively of the tuff of Rhyolite Ridge and rounded gray oncoidal limestone; distinctly Cambrian clasts are notably absent. Individual oncoids are up to 70 cm wide and oblate to spherical, reflecting their original shape. These strata are interpreted as debris-flow deposits that prograded into a shallow lacustrine setting; however, it is unclear whether these facies are correlative with the informally defined middle or upper members of the Cave Spring formation. Interbedded tuffs within sub-unit S3 have been dated at  $5.074 \pm 0.004$  Ma ( $^{40}\text{Ar}/^{39}\text{Ar}$ ; Chafetz, 2023) and  $4.73 \pm 0.08$  Ma (U-Pb; Ogilvie, 2023) (table 1). Total thickness of Tcsu is up to 250 m.

**Tcsm Middle member** Lacustrine marl, claystone, siltstone, carbonate with minor sandstone and gritstone that host economically significant lithium-boron ore zone. This informally named member corresponds with the S5, B5, M5, G5, and M4 sub-units of the Cave Spring formation defined by Reynolds and Chafetz (2020). The base of this middle member is composed of gray siltstone and interbedded fine gritstones with minor marl and claystone (S5). The overlying main ore zone consists of white to light green-gray or blue-gray finely laminated searlesite-bearing marls and clays (B5). This main ore zone grades into massive claystone with similar high grades of lithium (but lower boron) with a few thin gritstone marker beds, pink waxy smectite and irregular chalcedony lenses, with ripple laminations and sparse flute casts (M5). These main ore zone facies are abruptly overlain by a prominent volcaniclastic gritstone marker bed (G5) that is commonly oxidized orange from leaching by groundwater. The uppermost part of this section is composed of massive white carbonate and thinly bedded claystone and marl that contain a distinct black-and-white striped stromatolitic sequence (M4). Chafetz (2023) reports a  $^{40}\text{Ar}/^{39}\text{Ar}$  age of  $5.148 \pm 0.005$  Ma on a tuff/gritstone within sub-unit G5

(table 1). The total thickness of Tcsm ranges from 50 to 90 m.

**Tcls Lower member** Coarse conglomerates, gritstone, sandstone, limestone, and siltstone. This informally named member corresponds with the G7, L6, and G6 sub-units of the Cave Spring formation defined by Reynolds and Chafetz (2020). The base of this unit is typically characterized by either coarse, unsorted, diamictite and pebbly sandstone of variable thickness (up to 60 m) interpreted as debris flows, or massive clast-supported boulder breccias almost entirely of angular clasts of the tuff of Rhyolite Ridge (G7); it also contains megaporphyritic latite boulders up to 1.8 m in diameter derived from the immediately underlying Argentite Canyon formation (Tal) of Oldow et al. (2009). This basal diamictite facies is overlain in turn by a carbonate sequence consisting of thin-bedded lacustrine marl, algal limestone and stromatolitic bioherms, with lesser but distinctive light tan to black opaline and chalcedonic silica in its lower part (L6). The upper part of this member is defined by an orange-toned, oxidized volcaniclastic gritstone composed of locally coarse pumice that fines upward in a transition to siltstone (G6). Chafetz (2023) reported a  $^{40}\text{Ar}/^{39}\text{Ar}$  age of  $5.878 \pm 0.002$  Ma (table 1), which is statistically indistinguishable from the age of the underlying Argentite Canyon formation and thus constrains the maximum depositional age of this member. The total thickness of Tcls ranges from ~30 to 120 m.

**Ts Silver Peak formation (late to middle Miocene)** Interbedded, nonmarine, greenish-gray to green or tan tuffaceous and volcaniclastic sandstone, conglomerate, mudstone, and intercalated vitric tuffs. Coarser facies weather tan to rusty orange, form resistant ridges and cliffs, are generally well stratified and evenly bedded, and are more common in the western map area where clasts are dominantly volcanic in composition. Sandstones are moderately to poorly sorted, typically fine- to medium-grained, subangular to subrounded, and dominated by volcanic lithic fragments; normal grading and subtle low-angle cross-bedding are common. Some beds are distinctly non-volcanic and instead composed of quartz, chert, and sedimentary lithic fragments derived from Cambrian units. Mudstones are recessive and form poorly exposed slopes.

The Silver Peak formation has been extensively studied and has previously been referred to as either the “Esmeralda Formation” (Ferguson et al., 1953; Albers and Stewart, 1972; Stewart and Diamond, 1990; Diamond and Ingersoll, 2002)

“Sedimentary Unit 2” (Stewart et al., 1974), or “Sedimentary Unit 3” (Ts3; Robinson et al., 1976). Oldow et al. (2009) suggested abandoning the use of “Esmeralda Formation” based on its inconsistent and ambiguous use in the region and suggested the name “Silver Peak Formation” instead. Here, we follow Oldow et al. (2009) in adopting the informal name “Silver Peak formation” for this unit.

The base of the Silver Peak formation is constrained to be ~16.6 Ma based on the occurrence of freshwater mollusks and ostracods of Barstovian age (Robinson et al., 1968; Stewart and Diamond, 1990). It also contains several distinctive white vitric tuffs dated between 12.7 and 11.1 Ma (Robinson et al., 1968), and it is unconformably overlain by the 6.0 Ma tuff of Rhyolite Ridge (Robinson et al., 1976; Oldow et al., 2009). The Silver Peak formation rests unconformably on Cambrian basement units and the informally named Icehouse Canyon assemblage (Tic) of Oldow et al. (2009), and is widely interpreted as a supradetachment basin sequence deposited on the extending upper plate of the Silver Peak (or “Mineral Ridge”) detachment fault during middle to late Miocene time (Stewart and Diamond, 1990; Diamond and Ingersoll, 2002; Oldow et al., 2009). Total thickness is variable and ranges from ~200 to 1,200 m in the map area.

## Neogene Volcanic and Intrusive Rocks

**Tb Basalt flows (late Pliocene to late Miocene)** Uncommon black fresh to reddish-brown weathered basalt to trachybasalt lava flows. Lavas are typically microporphyritic and contain large (up to 7 mm) euhedral plagioclase phenocrysts with subordinate small (1–2 mm) clinopyroxene in a fine-grained plagioclase-rich groundmass. Some individual lavas also contain small, altered olivine phenocrysts and vesicular textures. Various basalt flows in Tb have been dated from ~4.8 to 3.7 Ma (table 1). Individual lavas are not laterally extensive along-strike and typically up to 5–8 m thick locally.

**Tbi Basaltic dikes and sills (late Pliocene to late Miocene)** Intrusive dikes and sills of mafic composition similar to Tb. Geochemically classified as mostly basalt and trachybasalt (fig. 4). Rare and isolated occurrences are laterally discontinuous and of limited extent. Two samples with anomalously high lithium concentrations of 151 and 451 ppm (fig. 5; table 2) may reflect artificial enrichment from associated host rocks. Most commonly observed intruding sharp depositional contacts at or near the base of the tuff of Rhyolite Ridge (Trt) and along short segments of

normal faults on the east side of the map area. Dikes are typically less than 3 m wide.

### Argentite Canyon formation (late Miocene)

The Argentite Canyon formation was informally named by Oldow et al. (2009) for a thick sequence of latite (or feldspar-rich trachyte) lava flows and pyroclastic rocks that are well exposed in the southeastern and south-central parts of the map area in Argentite Canyon, and throughout the topographically highest central part of Silver Peak Range. This unit was incorrectly interpreted by Oldow et al. (2009) as overlying the Cave Spring formation, which is refuted by extensive subsurface drilling and geochronology data that unequivocally indicate that 5.89-Ma Argentite Canyon formation is overlain by the Cave Spring formation, which contains numerous interbedded tuffs dated at ~5.8–4.7 Ma (Reynolds and Chafetz, 2020; Chafetz, 2023; Ogilvie, 2023) (fig. 3; table 1).

**Tat Welded rhyolitic ash-flow tuff** Pink, maroon or burnt orange, welded, crystal-rich, latite (trachyte to rhyolite; fig. 4) ash-flow tuff. Typically contains abundant diagnostic black, vitric pumice fiamme up to ~10 cm long that distinguish it from the underlying tuff of Rhyolite Ridge (Trt). Dark brownish-black desert varnish is common on weathered surfaces. The base of Tat is nonwelded to subwelded and contains mm-scale lithic fragments of tuff and light yellow to orange-pink pumice, and abundant phenocrysts (up to 25%) of mostly subhedral biotite, plagioclase, quartz and accessory clinopyroxene (Ogilvie, 2023). Welding is more intense upsection in the lower-middle part of the unit, which grades upward into a nonwelded and vapor-phase altered upper part with white to pale pink pumice. Whole-rock lithium concentrations range from 21–99 ppm for this unit (fig. 5). Tat was previously mapped as a latite welded tuff by Robinson et al. (1976; unit “Tlt”) who suggested a correlation with a similar welded tuff in the adjacent Piper Peak quadrangle dated at ~6.1 Ma [K-Ar]. More recently, this unit has been dated at  $5.87 \pm 0.02$  Ma (Oldow et al., 2009) to  $5.76 \pm 0.18$  Ma (Ogilvie, 2023) from exposures on the northern flanks of Rhyolite Ridge proper (table 1). Tat is only exposed to the north and east of Cave Spring, and most prominently along the crest and northwest flank of Rhyolite Ridge (*sensu stricto*) as a prominent dark brown layer that conformably overlies the lighter 6.0 Ma tuff of Rhyolite Ridge; small remnants are also mapped on Beacon Hill and along the eastern boundary of the

map near North Spring (fig. 2). Thickness varies from ~30 to 200 m.

**Tal Porphyritic latite lava flows** Porphyritic latite lavas and associated breccias make up the majority of the Argentite Canyon formation and form resistant cliffs in outcrop. Geochemically classified as latite (QAP classification of Streckeisen, 1978), or trachyandesite, trachydacite, or rhyolite (fig. 4; TAS classification of Le Bas et al., 1986). Typically dark brown on weathered surfaces; fresh surfaces range from having a dark gray to a dark pink or gray-green groundmass. Lavas characteristically contain 30–40% megacrystic potassium feldspar up to 4 cm long with minor (<5%) black to rusty biotite. Feldspar morphology ranges from anhedral to euhedral. Most potassium feldspar phenocrysts are anhedral or subhedral, and some display intergrowth and dissolution textures with opaque white plagioclase rims (Ogilvie, 2023) that suggest varying degrees of hydrothermal alteration. Whole-rock lithium concentrations mostly range from 159–358 ppm in this unit (fig. 5), substantially higher than typical rhyolites (e.g., Price et al., 2000). Tal conformably overlies the 6.0 Ma tuff of Rhyolite Ridge (Trt). A date from the upper part of Tal near its contact with the overlying Fish Lake Valley assemblage (Tf) in Wild Horse Canyon (fig. 2) yielded a sanidine  $^{40}\text{Ar}/^{39}\text{Ar}$  age of  $5.85 \pm 0.03$  Ma (Oldow et al., 2009). Thickness is highly variable and reaches a maximum of ~300 m in the map area.

**Tai Latite dikes and sills** Intrusive dikes and sills of latite (trachyte to rhyolite) that represent the magmatic plumbing system of the Argentite Canyon formation lavas (Tal). Best exposed at the south end of Wild Horse Canyon (fig. 2) where it consists of a linked network of relatively narrow dikes and sills, small intrusive pods, and an up to ~300-m-wide vertical feeder dike that intrudes the surrounding Silver Peak formation (Ts) (Ogilvie, 2023). Conspicuous subvertical foliations in the latite form sheer cliffs, especially near the margins of the intrusion. Where exposed, the contact with siltstone and medium-grained sandstone of the Silver Peak formation is indurated due to contact metamorphism. The edges of the intrusion display smaller, but still porphyritic phenocrysts of plagioclase compared to typical exposures of the Argentite Canyon latite, likely due to faster cooling along the dike margins. The main feeder dike system appears to connect with sub-horizontal extrusive latite flows (Tal) that overlie the tuff of Rhyolite Ridge on the surrounding ridgelines.

### Rhyolite Ridge formation (late Miocene)

The informal Rhyolite Ridge formation is informally named here for the voluminous sequence of rhyolite tuffs and lavas exposed at Rhyolite Ridge (*sensu stricto*) and throughout the Silver Peak Range. It is equivalent to the “Rhyolite Ridge Tuff” unit of Oldow et al. (2009), which is considered here to be a subunit of the Rhyolite Ridge formation, as described below. The Rhyolite Ridge formation unconformably overlies the Silver Peak formation or older Cambrian and Precambrian units in the vicinity of Mineral Ridge and the Silver Peak detachment fault in the northeastern map area. It is overlain in turn by the Argentite Canyon formation (Tal, Tat) and Cave Spring formation (Tcsl, Tcsm, Tcsu). Various age dates indicate an age of ~6.1–6.0 Ma for the Rhyolite Ridge formation (table 1), which is here divided into separate informal map units that are dominated either by nonwelded rhyolite tuff (Trt) and or by mixed facies of aphanitic rhyolite lavas and tuff breccias (Trlb). Excluding a few potentially spurious outliers, tuffs and lavas of the Rhyolite Ridge formation are mostly classified as rhyolites, dacites, and trachytes (fig. 4). The thickness of the Rhyolite Ridge formation varies throughout the study area and appears to reach a maximum composite thickness of ~525 m at Rhyolite Ridge.

**Trt Tuff of Rhyolite Ridge** Mostly light pink to white, beige, or light pistachio-green, lithic-rich, pumice- and lithic-rich, nonwelded rhyolitic ash-flow tuffs that make up the majority of the Rhyolite Ridge formation. Weathers light brown-beige to dark brown from desert varnish. Typically contains 5–10% (and up to 25%) phenocrysts of anhedral to subhedral quartz, oligoclase, sanidine, and minor biotite. Abundant pumice lapilli are light peach-pink, nonwelded, and range from ~2–30 mm in diameter. Abundant lithic fragments are typically very angular and composed of flow-banded red to black aphanitic rhyolite (Trlb), which make up >90% of the lithic fragments. Lithic fragments with perlitic texture are also present within the tuff but are not as common as flow-banded fragments. Uncommon blocks of similar rhyolite tuff and aphanitic rhyolite up to 1.5 m wide are locally entrained within the tuffs. In most areas, tuffs are internally massive and unsorted, poorly bedded, and relatively competent and form resistant cliffs and ridges. Trt is composed of at least 3 or 4 individual flow units that are each up to ~80 m thick and intercalated with subordinate rhyolite lavas and breccias that are mostly included in unit Trlb. Whole-rock lithium concentrations mostly range from 30–211 ppm in this unit (fig. 5), similar to significantly

higher than typical rhyolites (e.g., Price et al., 2000). Robinson et al. (1976) report a K-Ar age of ~6.0 Ma for the tuff of Rhyolite Ridge. Oldow et al. (2009) reported high-precision  $^{40}\text{Ar}/^{39}\text{Ar}$  dates on sanidine from several outcrops of Trt in the map area that indicate emplacement between  $6.09 \pm 0.03$  to  $6.02 \pm 0.03$  Ma (table 1).

**Trlb Rhyolite lavas, breccias, and tuff breccias** Mostly maroon to dark gray aphanitic trachyte to rhyolite lavas and breccias and interbedded green to grayish-tan tuff breccias that are interbedded with nonwelded tuffs of Trt. Lavas are generally 10–20 m thick and show characteristic black to gray vitric flow banding that locally displays mesoscale isoclinal and asymmetric folds (Ogilvie, 2023). Some tuff breccias and lavas are hydrothermally altered to a grayish-green and have a distinct perlitic texture throughout. Clasts within rhyolite breccias are angular pieces of flow-banded rhyolite that usually make up greater than 70% of the rock. Spherulitic lavas can be found down Argentite Canyon as well as near the northeast end of Rhyolite Ridge (fig. 2). Whole-rock lithium concentrations are typical and range from 19–60 ppm in this unit (fig. 5). Thickness is highly variable and typically ranges from 50 to 120 m.

**Tic Icehouse Canyon assemblage (middle to early Miocene)** Gray, blueish-gray, brown andesite lavas and breccias, pink to white dacitic to rhyolitic ash-flow tuffs and associated pyroclastic and volcaniclastic rocks. The unit was informally named by Oldow et al. (2009) after excellent and rare exposures of lower and middle Miocene volcanic strata in the northwest Silver Peak Range that are located immediately southwest of the map area. This unit only occurs in a few small areas on the extreme western, northern, and eastern margins of the map area, where it is dominantly composed of nonwelded, white to weathered reddish-pink, porphyritic dacitic ash-flow tuff. Subhedral to anhedral phenocrysts of quartz, feldspar, and biotite are common. K-Ar dates from Robinson et al. (1968) report K-Ar ages of ~21.5 and 22.8 Ma for ash-flow tuffs in this unit (table 1). The abundance of phenocrysts and relative lack of volcanic lithic fragments in tuffs of Tic help to distinguish them from the younger tuff of Rhyolite Ridge (Trt). Thickness is uncertain, but appears to be up to ~300 m in the map area.

## Paleozoic Metasedimentary Rocks

**Op Palmetto Formation (Ordovician)** Dark gray, grayish-green, and blueish-gray slaty shale and phyllite with

lesser limestone and black chert. Shale is platy, thinly laminated and recessive. Limestone beds are relatively resistant and thin to medium bedded. This unit is only exposed in a small area in the northwestern part of the map area, where it has a thickness of at least 100 m.

**Ec Emigrant Formation (Late to Middle Cambrian)** Interbedded gray, greenish-gray, and yellowish-brown shale, limestone, and cherty limestone. Typically displays even, thin to medium bedding. Thickness is uncertain, but likely no more than ~400 m in the map area.

**Cms Mule Spring Formation (Early Cambrian)** Cliff-forming, medium to dark gray, very thinly laminated carbonate with abundant white calcite veins. Bedding is typically thin to thick. Small, cm-scale concretionary algal structures (e.g., Girvanella sp.) are diagnostic of this unit in the study area (Robinson et al., 1976). Thickness varies from 20 to 80 m.

**Ch Harkless Formation (Early Cambrian)** Dark gray, brown and greenish-gray, fissile slate, phyllitic sandstone, siltstone, and quartzite. Sandstones are very fine grained to fine grained and well sorted. Less common black to dark gray limestone beds range up to 15 m thick and commonly display multiple generations of white coplanar to en échelon arrays of carbonate veins. Bedding is typically thin to laminated, platy, and even. Mica is especially abundant and visible along bedding planes. Total thickness does not exceed 250 m.

**Ep Poleta Formation (Early Cambrian)** Cliff-forming, massive, medium to dark gray limestone commonly containing abundant archaeocyathid fossils. In the middle of the unit, medium to thick limestones are interbedded with yellowish-brown to gray siltstone and dark gray fine-grained quartzite, and abundantly fossiliferous (Robinson et al., 1976). Thickness is up to 150 m.

**Cc Campito Formation (Early Cambrian)** Mostly brownish-gray to dark gray, medium to very thick-bedded, fine-grained quartzite with lesser dark green to greenish-gray phyllitic siltstone and sandstone. Only exposed along the northeast and northwest edge of the map. Thickness is at least 125 m.

## Metamorphic Rocks

**Zw Wyman Formation (late Neoproterozoic)** Heterolithic unit composed of dark brownish-gray to black and white schist, gneiss, calcschist, metacarbonate, and metasandstone. Moderately to strongly foliated and mylonitized, especially in close proximity to the Silver Peak–

Lone Mountain detachment fault. Mylonites contain blocky feldspar porphyroclasts set in a fine-grained matrix composed of biotite-amphibole-feldspar-quartz; uncommon asymmetric strain markers consistently indicate a top-to-west sense of shear. Locally displays ductile deformation structures such as small-scale parasitic folds and small-scale boudinage of more competent quartz-rich layers. Garnetiferous granite and pegmatite dikes and veins are common and both parallel and crosscut foliation. Granitic intrusions are related to emplacement of the ~55 Ma Mineral Ridge two-mica granite, which is exposed just east of the study area and occurs just below the Wyman Formation in the shallow subsurface across most of Mineral Ridge (Diamond and Ingersoll, 2002). The thickness of the Wyman Formation is uncertain but may be no more than ~300 m due to strong ductile attenuation during pluton emplacement.

## ACKNOWLEDGMENTS

This research and field work was supported by the U.S. Geological Survey, Earth Mapping Resources Initiative (Earth MRI) Program and National Cooperative Geologic Mapping Program, under USGS award number G21AC10365, and by a graduate student research grant to I. Ogilvie from the Geological Society of America. The views and conclusions contained in this document are those of the authors and should not be interpreted as necessarily representing the official policies, either expressed or implied, of the U.S. Government. We are especially grateful to Ioneer USA Corporation for logistical assistance and for generously providing valuable geologic data and notes from their mapping, subsurface drilling, core samples, and remote sensing datasets, all of which greatly improved our understanding of the geology and the accuracy of the geologic map. Many thanks to Mary Hannah Giddens, Wes Johns, Rachel Micander, and Dominik Vlaha for their valuable assistance in the field. Thanks to Racheal Johnson for sharing field notes and data with us, and to Chris Henry for valuable discussions that improved this work.

## REFERENCES

- Albers, J.P., and Stewart, J.H., 1972, Geologic map of Esmeralda County, Nevada: Nevada Bureau of Mines and Geology Bulletin 78, scale 1:250,000.
- Angster, S.J., Wesnousky, S.G., Figueriredo, P.M., Owen, L.A., and Hammer, S.J., 2019, Late Quaternary slip rates for faults of the central Walker Lane (Nevada, USA): Spatiotemporal strain release in a strike-slip fault system: *Geosphere*, v. 15, no. 5, p. 1460-1478.

Bennett, R.A., Wernicke, B.P., Niemi, N.A., Friedrich, A.M., and Davis, J.L., 2003, Contemporary strain rates in the northern Basin and Range Province from GPS data: *Tectonics*, v. 22(2), 31 p.

Chafetz, D., 2023, Mineralogy and geochemistry of a lithium and boron enriched stratiform ore zone in the Cave Spring Formation, Rhyolite Ridge, NV, USA: University of Nevada, Reno, M.S. thesis, 619p.

Diamond, D.S., and Ingersoll, R.A., 2002, Structural and sedimentologic evolution of a Miocene supradetachment basin, Silver Peak Range and adjacent areas, west-central Nevada: *International Geology Review*, v. 44, p. 588–623, <https://doi.org/10.2747/0020-6814.44.7.588>.

Dokka, R.K., and Travis, C.J., 1990, Role of the eastern California shear zone in accommodating Pacific-North American plate motion: *Geophysical Research Letters*, v. 17(9), p. 1323–1326.

Faulds, J.E., and Henry, C.D., 2008, Tectonic influences on the spatial and temporal evolution of the Walker Lane—an incipient transform fault along the evolving Pacific-North American plate boundary, in Spencer, J.E., and Titley, S.R., editors, *Ores and orogenesis: Circum-Pacific tectonics, geologic evolution, and ore deposits*: Arizona Geological Society Digest 22, p. 437–470.

Ferguson, H.G., Muller, S.W., and Cathcart, S., 1953, Geology of the Coaldale quadrangle, Nevada: U.S. Geological Survey Map GQ-23, scale 1:125,000.

Hammond, W.C., Blewitt, G., Kreemer, C., Koehler, R.D., and Dee, S., 2020, Geodetic observation of seismic cycles before, during, and after the 2020 Monte Cristo Range, Nevada earthquake: *Seismological Research Letters*, <https://doi.org/10.1785/0220200338>.

Hoeft, J.S., and Frankel, K.L., 2012, Preliminary surficial geologic map along the northwest Lone Mountain and Weepah Hills piedmonts, Esmeralda County, Nevada: Nevada Bureau of Mines and Geology Open-File Report 2012-01, scale 1:24,000.

Koehler, R.D., Dee, S., Elliott, A., Hatem, A., Pickering, A., Pierce, I., and Seitz, G., 2021, Field response and surface-rupture characteristics of the 2020 M 6.5 Monte Cristo Range earthquake, central Walker Lane, Nevada: *Seismological Research Letters*, <https://doi.org/10.1785/0220200371>.

Le Bas, M.J., Le Maitre, R.W., Streckeisen, A., and Zanettin, B., 1986, A chemical classification of volcanic rocks based on the total alkali-silica diagram: *Journal of Petrology*, v. 27, no. 3, p. 745–750.

Lifton, Z.M., Newman, A.V., Frankel, K.L., Johnson, C.W., and Dixon, T.H., 2013, Insights into distributed plate rates across the Walker Lane from GPS geodesy: *Geophysical Research Letters*, v. 40(17), p. 4620–4624.

Maldonado, F., 1990, Geologic map of the northwest quarter of the Bullfrog 15-minute quadrangle, Nye County, Nevada: U.S. Geological Survey Miscellaneous Investigations Series Map I-1985, scale, 1:24,000, <https://doi.org/10.3133/i1985>.

- McKee, E.H., Diggles, M.F., Donahoe, J.L., and Elliot, G.S., 1982, Geologic map of the White Mountains Wilderness and roadless areas, California and Nevada: U.S. Geological Survey Miscellaneous Field Studies Map MF-1361-A, scale 1:62,500.
- McKee, E.H., 1985, Geologic map of the Magruder Mountain quadrangle, Esmeralda County, Nevada, and Inyo County, California: U.S. Geological Survey Map GQ-1587, scale 1:62,500.
- Ogilvie I.A., 2023, Structure, stratigraphy, and source of sediment-hosted lithium deposits at Rhyolite Ridge, Silver Peak Range, western Nevada: University of Nevada, Reno, M.S. thesis, 153 p.
- Oldow, J.S., Elias, E.A., Ferranti, L., McClelland, W.C., McIntosh, W.C., and Cashman, P.H., 2009, Late Miocene to Pliocene synextensional deposition in fault-bounded basins within the upper plate of the western Silver Peak–Lone Mountain extensional complex, west-central Nevada, *in* Oldow, J.S. and Cashman, P.H., editors, Late Cenozoic structure and evolution of the Great Basin–Sierra Nevada transition: Geological Society of America Special Paper 447, p. 275–312.
- Petronis, M.S., Geissman, J.W., Oldow, J.S., and McIntosh, W.C., 2002, Paleomagnetic and  $^{40}\text{Ar}/^{39}\text{Ar}$  geochronologic data bearing on the structural evolution of the Silver Peak extensional complex, west-central Nevada: Geological Society of America Bulletin, v. 114, no. 9, p. 1108–1130.
- Price, J.G., Lechler, P.J., Lear, M.B., and Giles, T.F., 2000, Possible volcanic source of lithium in brines in Clayton Valley, Nevada, *in* Cluer, J.K., Price, J.G., Struhsacker, E.M., Hardymann, R.F., and Morris, C.L., editors, Geology and ore deposits 2000—the Great Basin and Beyond: Geological Society of Nevada Symposium Proceedings, May 15–18, 2000, p. 241–248.
- Reheis, M.C., 1991, Geologic map of late Cenozoic deposits and faults in the western part of the Rhyolite Ridge 15' quadrangle, Esmeralda County, Nevada: U.S. Geological Survey Miscellaneous Investigations Series Map I-2183, scale 1:24,000.
- Reheis, M.C., and Sawyer, T.L., 1997, Late Cenozoic history and slip rates of the Fish Lake Valley, Emigrant Peak, and Deep Springs fault zones, Nevada and California: Geological Society of America Bulletin, v. 109, no. 3, p. 280–299.
- Reheis, M.C., Sawyer, T.L., Slate, J.L., and Gillespie, A.R., 1993, Geologic map of late Cenozoic deposits and faults in the southern part of the Davis Mountain 15' quadrangle, Esmeralda County, Nevada: U.S. Geological Survey Miscellaneous Investigations Series Map I-2342, scale 1:24,000.
- Reynolds, J.T., and Chafetz, D.A., 2020, Geology of the lithium-boron Rhyolite Ridge project, Silver Peak Range, Esmeralda County, Nevada: Reno, Geological Society of Nevada Symposium, p. 435–450.
- Robinson, P.T., and Crowder, D.F., 1973, Geologic map of the Davis Mountain quadrangle, Esmeralda and Mineral counties, Nevada, and Mono County, California: U.S. Geological Survey Map GQ-1078, scale 1:62,500.
- Robinson, P.T., McKee, E.H., and Moiola, R.J., 1968, Cenozoic volcanism and sedimentation, Silver Peak region, western Nevada and adjacent California, *in* Coats, R.R., Hay, R.L., and Anderson, C.A., editors, Studies in volcanology—a memoir in honor of Howell Williams: Geological Society of America Memoir 116, p. 577–611.
- Robinson, P.T., Stewart, J.H., Moiola, R.J., and Albers, J.P., 1976, Geologic map of the Rhyolite Ridge quadrangle, Esmeralda County: Nevada, U.S. Geological Survey Map GQ-1325, scale 1:62,500.
- Stewart, J.H., and Diamond, D.S., 1990, Changing patterns of extensional tectonics—overprinting of the basin of the middle and upper Miocene Esmeralda Formation in western Nevada by younger structural basins: Geological Society of America Memoir 176, p. 447–476.
- Stewart, J.H., Robinson, P.T., Albers, J.P., and Crowder, D.F., 1974, Geologic map of the Piper Peak quadrangle, Nevada-California, U.S. Geological Survey Map GQ-1186, scale 1:62,500.
- Stewart, J.H., Kelleher, P.C., and Zorich, E.A., 1994, Geologic map of the Monte Cristo Range area, Esmeralda and Mineral counties, Nevada: U.S. Geological Survey, Miscellaneous Field Studies Map MF-2260, scale 1:62,500.
- Streckeisen, A., 1978, IUGS Subcommission on the systematics of igneous rocks—classification and nomenclature of volcanic rocks, lamprophyres, carbonatites, and melilite rocks: Recommendations and suggestions: Neues Jahrbuch für Mineralogie, Stuttgart, Abhandlungen, Germany, v. 143, p. 1–14. ISSN 0077-7757.

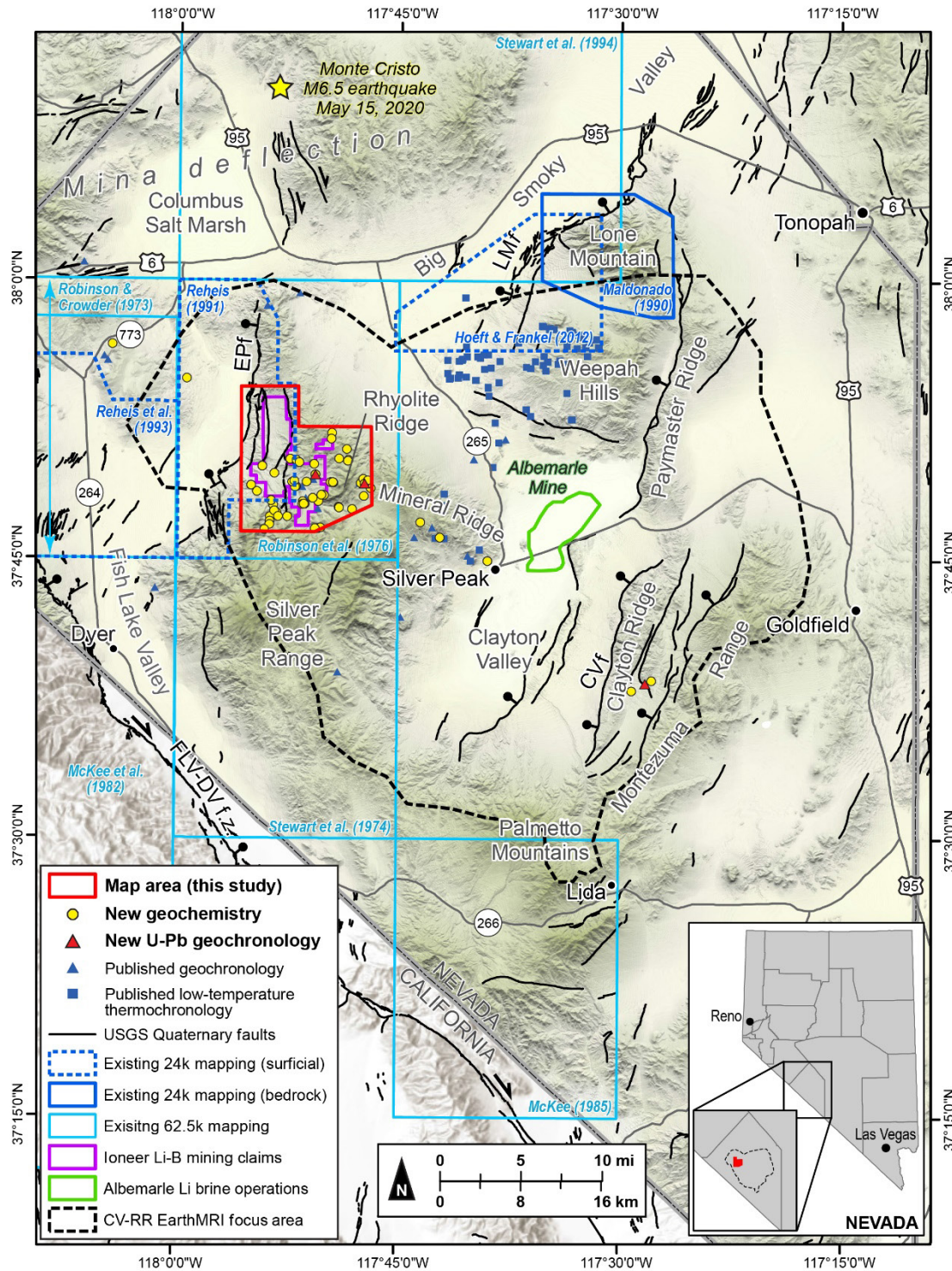


**Figure 1.** Location map and tectonic setting of the Rhyolite Ridge study area within the Clayton Valley–Rhyolite Ridge (CV-RR) Earth MRI focus area (dashed black line). Red outline indicates extent of 1:24,000-scale geologic mapping in this study. The extents of published geologic maps (blue), locations of active lithium (Li) brine operations by Albemarle (green) and sediment-hosted lithium (Li) and boron (B) deposits and claims under development by Ioneer USA Corp. (purple) are also highlighted. CVf – Clayton Valley fault; EPf – Emigrant Peak fault; FLV-DV f.z. – Fish Lake–Death Valley fault zone.

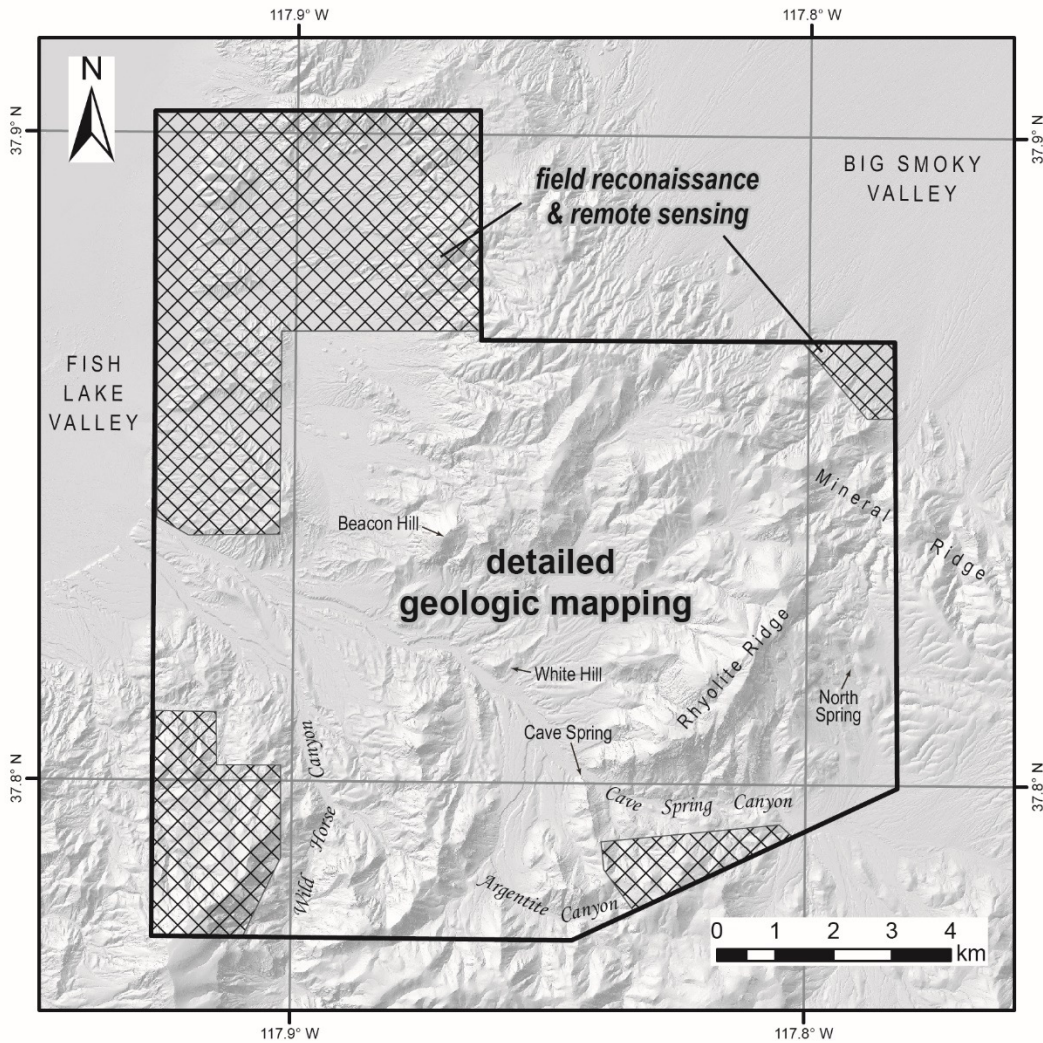


**Figure 2.** Data quality reference map for the Rhyolite Ridge study area. Unhatched areas within the black map boundary were mapped in greater detail, while only reconnaissance mapping was conducted in hatched areas. Mapping across the entire study area benefited from multiple remote sensing and aerial imagery datasets including high-resolution (<1 m/pixel) QL2 LiDAR elevation data and unpublished airborne electromagnetic resistivity data that were both acquired through the Geoscience Data Acquisition for Western Nevada (GeoDAWN) program funded through the USGS Earth MRI, as well as orthorectified, hyperspectral WorldView-3 satellite imagery provided by Ioneer USA Corporation.

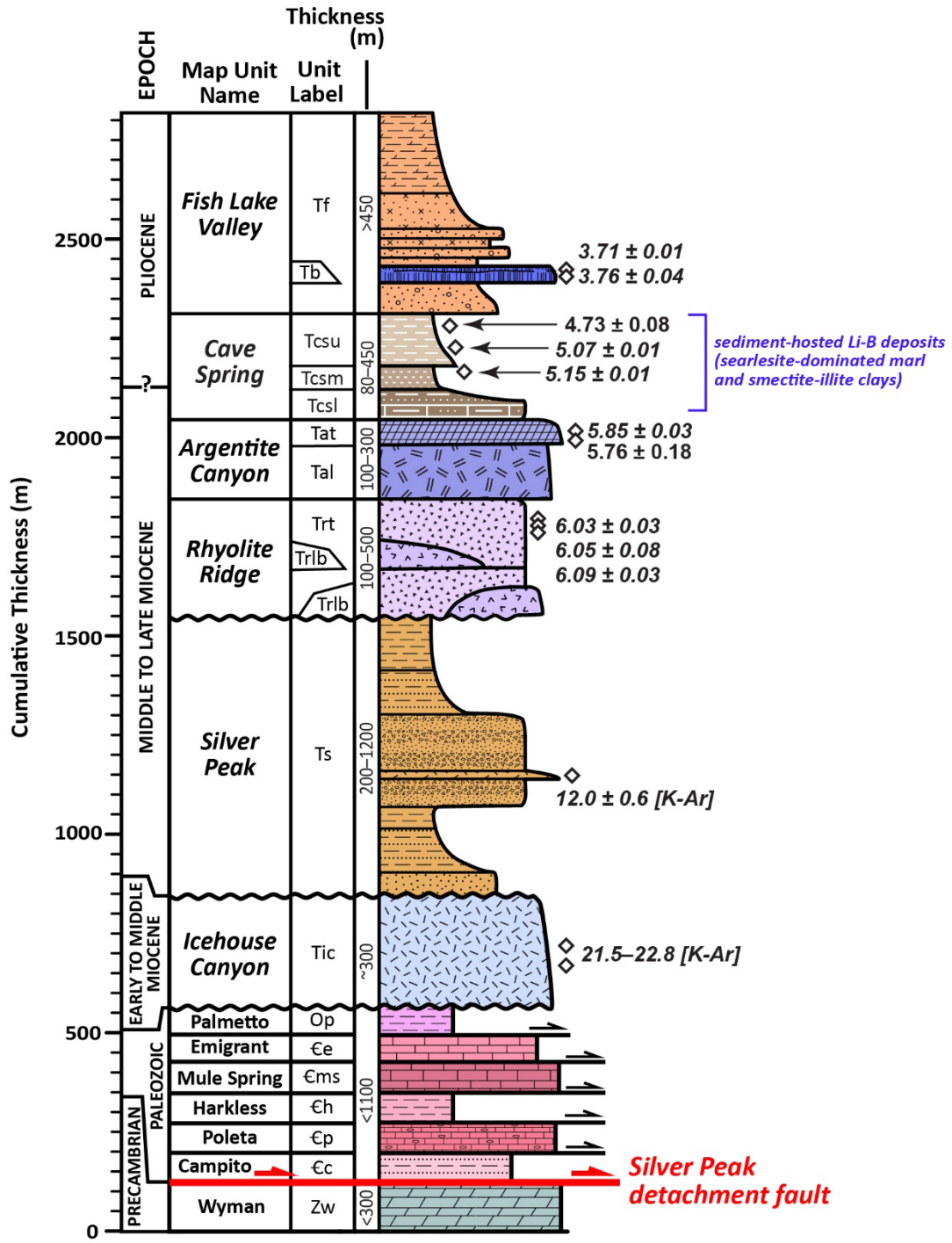


**Figure 3.** Composite stratigraphic column for the Rhyolite Ridge study area and northern Silver Peak Range adapted from Ogilvie (2023) and excluding Tertiary intrusive and Quaternary map units. Informal map unit names are shown in italics. Diamonds indicate published geochronology data after Robinson et al. (1976), Stewart and Diamond (1990), Oldow et al. (2009), Chafetz (2023), and Ogilvie (2023). All ages are reported in Ma with  $\pm 2\sigma$  errors, where available (table 1). The thicknesses of Precambrian and Paleozoic units are highly variable (~20–400 m each) due to extreme structural attenuation, and thus are only shown schematically here.

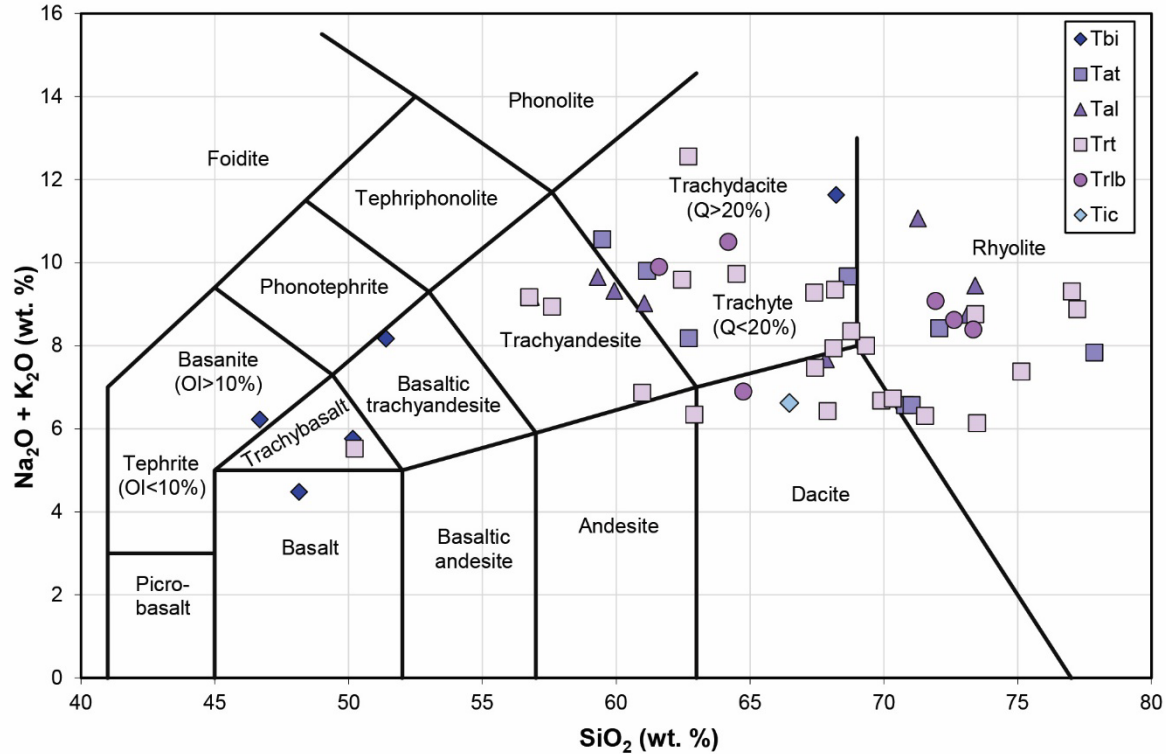


**Figure 4.** Total alkali-silica (TAS) diagram (Le Bas et al., 1986) showing general classifications of Neogene igneous rocks in the study area including the Icehouse Canyon assemblage (Tic), Rhyolite Ridge formation tuff (Trt) and lavas (Trlb), Argentite Canyon formation lavas (Tal) and welded rhyolitic ash-flow tuff (Tat), and Pliocene mafic intrusions (Tbi). Ol – olivine; Q – quartz.

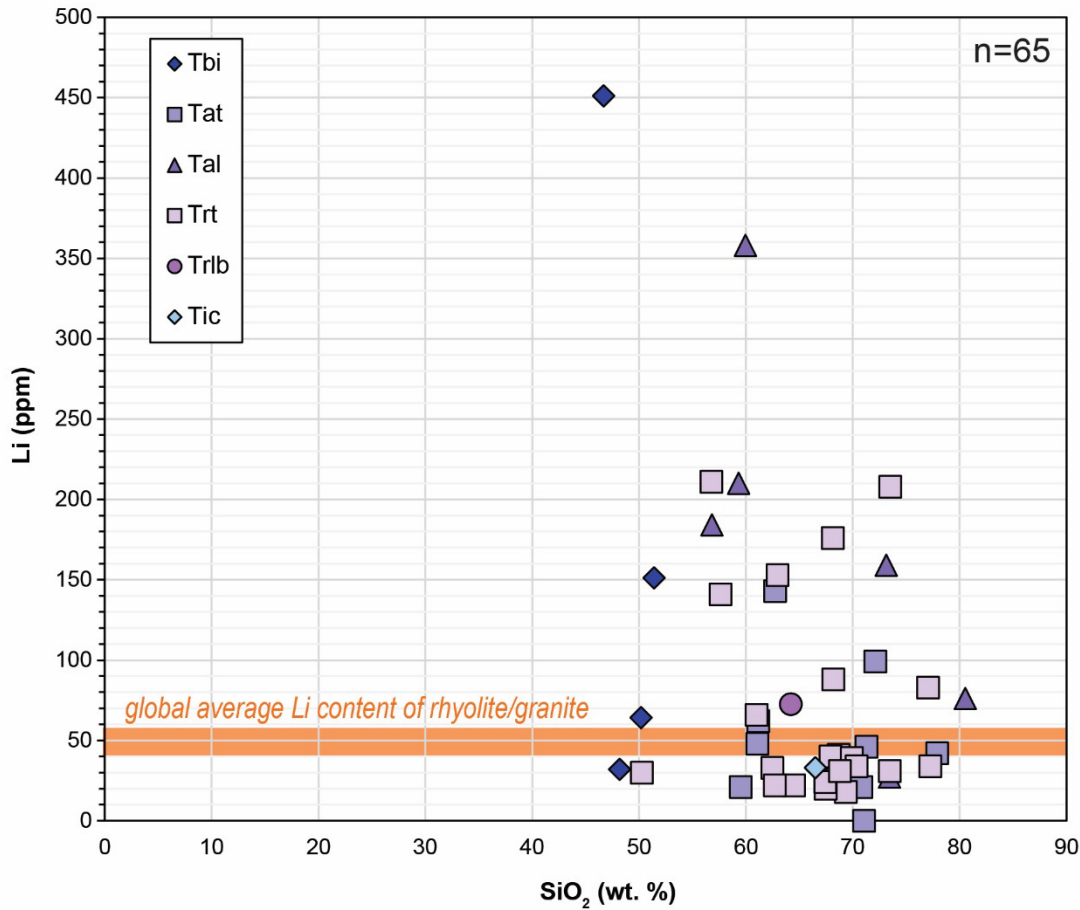


**Figure 5.** Whole-rock geochemical data from volcanic and sub-volcanic units in the study area, including the Icehouse Canyon assemblage (Tic), Rhyolite Ridge formation tuff (Trt) and lavas (Trlb), Argentite Canyon formation lavas (Tal) and welded rhyolitic ash-flow tuff (Tat), and Pliocene mafic intrusions (Tbi). Many samples from the Rhyolite Ridge and Argentite Canyon formations have anomalously high lithium (Li) concentrations up to 451 ppm. These lithium concentrations at Rhyolite Ridge are substantially higher than average values of only 40–58 ppm for granites and rhyolites based on a global data compilation that excludes one outlier from Peru with 3,400 ppm lithium (Price et al., 2000, and references therein).

**Table 1.** Compilation of published geochronologic data from the greater Rhyolite Ridge study area. (Samples names in italic are not shown on map.)

Sample	Formation	Latitude	Longitude	Lithology	Material	Method	Age (Ma)	$\pm 2\sigma$ (Ma)	Reference	Notes
<b>102801-1a</b>	Fish Lake Valley	37.7985	-117.8925	basalt	groundmass	Ar/Ar	<b>3.71</b>	<b>0.01</b>	Oldow et al. (2009)	
<b>102803-1b</b>	Fish Lake Valley	37.79855	-117.89255	basalt	groundmass	Ar/Ar	<b>3.76</b>	<b>0.04</b>	Oldow et al. (2009)	
<i>7</i>	Pliocene basalt flows (Tb)	37.724193	-118.025713	basalt	whole rock	K-Ar	<b>4.8</b>	<b>1.2</b>	Robinson et al. (1968)	location approximate
<b>RRIO21-27</b>	Cave Spring	37.826586	-117.845545	tuff	zircon	U-Pb	<b>4.73</b>	<b>0.08</b>	Ogilvie (2023)	
<b>DCC-025</b>	Cave Spring	37.805657	-117.856385	tuff/grit	sanidine	Ar/Ar	<b>5.074</b>	<b>0.004</b>	Chaffetz (2023)	drill core sample
<b>DCC-018</b>	Cave Spring	37.822147	-117.848167	tuff/grit	sanidine	Ar/Ar	<b>5.148</b>	<b>0.005</b>	Chaffetz (2023)	drill core sample
<b>DCC-056</b>	Cave Spring	37.80209	-117.857321	tuff/grit	sanidine	Ar/Ar	<b>5.878</b>	<b>0.002</b>	Chaffetz (2023)	drill core sample
<b>MD22RR-128</b>	Argentite Canyon	37.818863	-117.790205	welded tuff	zircon	U-Pb	<b>5.76</b>	<b>0.18</b>	Ogilvie (2023)	
<b>102803-2</b>	Argentite Canyon	37.805	-117.897167	welded tuff	sanidine	Ar/Ar	<b>5.85</b>	<b>0.03</b>	Oldow et al. (2009)	
<b>102703-5</b>	Argentite Canyon	37.841	-117.666833	welded tuff	sanidine	Ar/Ar	<b>5.87</b>	<b>0.02</b>	Oldow et al. (2009)	
<i>5</i>	Argentite Canyon	37.64993	-117.818961	welded tuff	biotite	K-Ar	<b>6.1</b>	<b>0.6</b>	Robinson et al. (1968)	location approximate
<i>8</i>	Argentite Canyon	37.699394	-117.748365	trachy-andesite lava	biotite	K-Ar	<b>5.9</b>	<b>0.4</b>	Robinson et al. (1968)	location approximate
<b>RRIO22-64</b>	Rhyolite Ridge	37.640368	-117.472324	tuff	zircon	U-Pb	<b>6.05</b>	<b>0.08</b>	Ogilvie (2023)	
<b>102703-4</b>	Rhyolite Ridge	37.84105	-117.666667	tuff	sanidine	Ar/Ar	<b>6.03</b>	<b>0.03</b>	Oldow et al. (2009)	
<b>102403-3</b>	Rhyolite Ridge	37.8195	-117.795833	tuff	sanidine	Ar/Ar	<b>6.09</b>	<b>0.03</b>	Oldow et al. (2009)	
<b>102903-1</b>	Rhyolite Ridge	37.815833	-117.860333	tuff	sanidine	Ar/Ar	<b>6.02</b>	<b>0.03</b>	Oldow et al. (2009)	
<i>6</i>	Rhyolite Ridge	37.796102	-117.842663	tuff	biotite	K-Ar	<b>6.0</b>	<b>1.0</b>	Robinson et al. (1968)	location approximate
<i>13</i>	Rhyolite Ridge	37.859161	-117.631201	tuff	biotite	K-Ar	<b>6.9</b>	<b>0.6</b>	Robinson et al. (1968)	location approximate
<i>2</i>	Rhyolite Ridge?	37.368336	-117.799232	tuff	biotite	K-Ar	<b>4.3</b>	<b>0.8</b>	Robinson et al. (1968)	location approximate
<i>3</i>	Rhyolite Ridge?	37.342838	-117.840537	tuff	biotite	K-Ar	<b>5.7</b>	<b>1.2</b>	Robinson et al. (1968)	location approximate
<i>4</i>	Silver Peak?	37.380846	-117.864810	welded tuff	sanidine	K-Ar	<b>8.2</b>	<b>0.4</b>	Robinson et al. (1968)	location approximate
<i>9</i>	Silver Peak	37.932089	-118.085383	tuff	biotite	K-Ar	<b>11.1</b>	<b>0.4</b>	Robinson et al. (1968)	location approximate
<i>10</i>	Silver Peak	37.928055	-118.081300	tuff	biotite	K-Ar	<b>11.4</b>	<b>0.4</b>	Robinson et al. (1968)	location approximate
<i>11</i>	Silver Peak	37.989366	-117.864765	tuff	biotite	K-Ar	<b>12.7</b>	<b>0.4</b>	Robinson et al. (1968)	location approximate
<i>1</i>	Silver Peak	37.366542	-117.794036	tuff	biotite	K-Ar	<b>13.1</b>	<b>1.6</b>	Robinson et al. (1968)	location approximate
<i>12</i>	Icehouse Canyon	37.978068	-117.901330	welded tuff	biotite	K-Ar	<b>21.5</b>	<b>2.0</b>	Robinson et al. (1968)	location approximate
<i>14</i>	Icehouse Canyon	38.015942	-118.109659	welded tuff	biotite	K-Ar	<b>22.8</b>	<b>2.0</b>	Robinson et al. (1968)	location approximate
<b>SP-55</b>	--	37.770882	-117.733701	mafic dike	groundmass	Ar/Ar	<b>11.6</b>	<b>0.4</b>	Petronis et al. (2002)	
<b>SP-69</b>	--	37.754581	-117.673334	mafic dike	groundmass	Ar/Ar	<b>11.4</b>	<b>0.6</b>	Petronis et al. (2002)	
<b>SP-75</b>	--	37.754581	-117.673334	mafic dike	groundmass	Ar/Ar	<b>11.3</b>	<b>0.2</b>	Petronis et al. (2002)	
<b>SP-92</b>	--	37.80	-117.7	mafic dike	groundmass	Ar/Ar	<b>10.5</b>	<b>0.8</b>	Petronis et al. (2002)	
<b>SP-96</b>	--	37.80	-117.7	mafic dike	groundmass	Ar/Ar	<b>12.4</b>	<b>1.9</b>	Petronis et al. (2002)	
<b>SP-112</b>	--	37.779765	-117.713450	mafic dike	groundmass	Ar/Ar	<b>10.9</b>	<b>0.3</b>	Petronis et al. (2002)	

**Table 2.** New whole-rock geochemical data from the greater Rhyolite Ridge study area.

Sample	RRIO21-3	RRIO21-37	RRIO21-39	RRSBHC10-613	RRIO22-48	RRSBH84-393	RRIO21-29
Latitude	37.815901	37.799234	37.792264	37.805644	37.849641	37.800172	37.802544
Longitude	-117.867375	-117.893148	-117.889008	-117.8484	-117.810242	-117.857272	-117.842245
Map Unit	Ts	Tf	Ts	Trt	Tbi	Tal	Trt
Lithology	rhyolitic tuff	reworked tuff	siltstone	rhyolitic tuff	basaltic sill	latite	rhyolitic tuff
<b>Major elements (wt %)</b>							
SiO <sub>2</sub>	1.02	12.83	12.82	71.03	46.68	59.93	56.74
TiO <sub>2</sub>	0.02	0.04	0.04	0.11	1.13	0.7	0.91
Al <sub>2</sub> O <sub>3</sub>	0.35	1.21	1.24	11.85	20.52	15.97	17.88
Fe <sub>2</sub> O <sub>3</sub>	0.31	0.29	0.29	0.73	6.31	4.26	4.98
MnO	0.02	0.28	0.28	0.05	0.17	0.07	0.1
MgO	21.03	0.32	0.31	0.24	2.46	2.22	1.41
CaO	30.28	47.3	47.22	1.18	10.11	3.31	4.58
Na <sub>2</sub> O	<0.01	0.04	0.07	3.12	4.12	3.86	2.44
K <sub>2</sub> O	0.1	0.41	0.48	3.45	2.1	5.46	6.73
P <sub>2</sub> O <sub>5</sub>	<0.01	0.05	0.05	0.01	0.57	0.28	0.37
SrO	<0.01	0.09	0.08	0.05	--	--	0.1
BaO	<0.01	0.05	0.04	0.02	0.16	0.16	0.23
V <sub>2</sub> O <sub>5</sub>	<0.01	<0.01	<0.01	<0.01	0.03	0.02	0.01
Cr <sub>2</sub> O <sub>3</sub>	<0.01	<0.01	<0.01	<0.01	<0.01	<0.01	<0.01
LOI*	46.47	37.27	37.09	8.06	5.49	3.9604	3.6
Total	99.60	100.18	100.01	99.90	99.85	100.20	100.08
<b>Minor and trace elements (ppm)</b>							
Ag	<1	<1	<1	<1	<1	<1	<1
As	<5	<5	<5	6	13	421	12
B	<10	<10	<10	29	139	128	220
Ba	5.2	360	403	161	1303	1294	1890
Be	<5	<5	<5	<5	<5	<5	<5
Bi	<0.1	<0.1	<0.1	0.2	<0.1	<0.1	<0.1
Cd	<0.2	<0.2	<0.2	<0.2	<0.2	<0.2	<0.2
Ce	3.8	8.8	9	43.1	74.2	104	111
Co	1.1	1.2	1.3	<0.5	25.7	8.4	9.5
Cr	14	24	10	13	26	16	29
Cs	0.2	4.8	4.6	121	77.5	18.4	30
Cu	<5	<5	<5	<5	21	<10	9
Dy	0.62	0.36	0.38	0.72	3.7	3.77	3.67
Er	0.44	0.27	0.26	0.64	1.98	2.15	1.9
Eu	0.11	0.1	0.09	0.15	1.81	1.35	1.66
Ga	0.41	1.19	1.32	15	21	19	17.9
Gd	0.69	0.38	0.39	0.67	5.18	4.51	4.83
Ge	<1	<1	<1	1	2	3	2
Hf	<1	<1	<1	3	4	8	7
Ho	0.13	0.08	0.09	0.16	0.72	0.76	0.63
In	<0.2	<0.2	<0.2	<0.2	<0.2	<0.2	<0.2
La	5.5	4.8	4.9	31.2	36.3	54.8	56.6
Li	<10	<10	<10	<10	451	358	211
Lu	<0.05	0.06	0.06	0.19	0.26	0.38	0.26
Mn	137	2230	2580	344	1345	561	936
Mo	<2	2	2	<2	<2	9	<2
Nb	0.2	2.6	2.3	15.5	11	24	13.4
Nd	3.1	2.9	2.9	7.8	38.8	41	41.4
Ni	<5	<5	<5	<5	32	16	<5
Pb	<5	<5	<5	28	8	21	20
Pr	0.79	0.84	0.83	3.14	9.71	11.78	11.3
Rb	2.8	16.2	18.7	301	44.1	167	191

<b>Sample</b>	<b>RRIO21-3</b>	<b>RRIO21-37</b>	<b>RRIO21-39</b>	<b>RRSBHC10-613</b>	<b>RRIO22-48</b>	<b>RRSBH84-393</b>	<b>RRIO21-29</b>
<b>Re</b>	<0.02	<0.02	<0.02	<0.02	<0.02	<0.02	<0.02
<b>Sb</b>	<0.1	3.4	3.4	0.9	0.4	14.8	1
<b>Sc</b>	<5	<5	<5	<5	19	7	10
<b>Se</b>	<5	<5	<5	<5	<1	<1	<5
<b>Sm</b>	0.5	0.5	0.5	0.9	6.6	6.4	6.7
<b>Sn</b>	<1	<1	<1	<1	1	<1	1
<b>Sr</b>	73.6	762	839	459	1194	652	954
<b>Ta</b>	<0.5	<0.5	<0.5	1	<0.5	0.9	1.1
<b>Tb</b>	0.09	0.06	0.06	0.1	0.7	0.67	0.63
<b>Te</b>	<0.5	<0.5	<0.5	<0.5	<0.05	<0.05	<0.5
<b>Th</b>	0.3	1.2	1.2	20.7	3.8	14.4	8.7
<b>Tl</b>	<0.5	11.3	11.2	2	<0.5	<0.5	<0.5
<b>Tm</b>	0.06	<0.05	<0.05	0.13	0.27	0.34	0.25
<b>U</b>	0.15	6.82	7.02	5.59	1.11	6.01	1.74
<b>V</b>	20	40	37	<5	195	79	81
<b>W</b>	<1	1	1	2	2	3	3
<b>Y</b>	7.7	3	2.8	6.2	17.2	19.7	17.4
<b>Yb</b>	0.3	0.3	0.3	1.1	1.7	2.4	1.8
<b>Zn</b>	<5	11	18	25	78	68	83
<b>Zr</b>	5.8	22.4	26.3	78.2	158	331	245

**Table 2.** New whole-rock geochemical data from the greater Rhyolite Ridge study area (continued).

Sample	RRSBH52-562	RRIO21-28	RRIO21-16	RRIO22-64	RRIO21-20	RRMH21-6	RRMD21-4
Latitude	37.802594	37.83596	37.778295	37.640368	37.819307	37.799923	37.819559
Longitude	-117.859685	-117.847066	-117.842504	-117.472324	-117.794524	-117.860138	-117.825305
Map Unit	Tal	Trt	Tal	Trt	Ts	Tal	Trt
Lithology	latite	rhyolitic tuff	latite	rhyolitic tuff	rhyolitic tuff	latite	rhyolitic tuff
<b>Major elements (wt %)</b>							
SiO <sub>2</sub>	59.3	73.48	56.81	68.11	81.3	73.11	62.91
TiO <sub>2</sub>	0.91	0.09	0.9	0.25	0.08	0.46	0.45
Al <sub>2</sub> O <sub>3</sub>	16.96	11.4	17.82	13.69	9.58	12	14.57
Fe <sub>2</sub> O <sub>3</sub>	4.66	0.65	4.92	1.63	0.61	2.2	2.89
MnO	0.05	0.05	0.11	0.07	0.04	0.01	0.07
MgO	1.51	0.55	1.4	0.94	0.11	0.7	1.4
CaO	3.42	1.42	4.6	1.83	0.19	0.25	4.71
Na <sub>2</sub> O	3.87	3.1	2.44	2.81	1.66	0.81	2.55
K <sub>2</sub> O	5.78	3.04	6.73	5.13	5.67	7.93	3.79
P <sub>2</sub> O <sub>5</sub>	0.43	0.02	0.36	0.05	<0.01	0.04	0.13
SrO	--	0.03	0.11	--	<0.01	0.01	0.06
BaO	0.17	0.02	0.22	0.03	<0.01	0.04	0.1
V <sub>2</sub> O <sub>5</sub>	0.02	<0.01	0.02	<0.01	<0.01	0.01	0.01
Cr <sub>2</sub> O <sub>3</sub>	<0.01	<0.01	<0.01	<0.01	<0.01	<0.01	<0.01
LOI*	2.45025	6.12	3.6	5.69	0.49	2.29	6.31
Total	99.53	99.97	100.04	100.23	99.73	99.86	99.95
<b>Minor and trace elements (ppm)</b>							
Ag	<1	<1	<1	<1	<1	<1	<1
As	55	5	12	6	11	59	20
B	78	64	239	62	69	487	102
Ba	1508	105	1830	252	73.9	413	758
Be	<5	6	<5	<5	<5	<5	<5
Bi	<0.1	0.3	<0.1	0.1	<0.1	0.2	0.2
Cd	<0.2	<0.2	<0.2	<0.2	<0.2	<0.2	<0.2
Ce	115	42.2	114	80.9	36.5	53.5	76.7
Co	10.5	1.1	9.6	1.8	<0.5	2.8	7.2
Cr	18	17	24	<10	14	52	54
Cs	22.9	17.8	30.1	14.2	4.2	312	12.4
Cu	26	<5	7	<10	7	<5	9
Dy	4.02	1.88	3.64	3.2	0.63	1.42	3
Er	2.27	1.44	1.87	2.01	0.46	0.71	1.91
Eu	1.6	0.1	1.55	0.59	0.12	0.71	0.93
Ga	19	16.4	17.4	17	12.7	13.8	17.9
Gd	5.02	1.78	5.06	3.6	0.63	2.12	3.63
Ge	3	2	2	1	2	5	3
Hf	7	4	7	6	2	4	6
Ho	0.8	0.42	0.64	0.66	0.13	0.24	0.62
In	<0.2	<0.2	<0.2	<0.2	<0.2	<0.2	<0.2
La	60.6	22.2	58.1	45.9	26.4	29	42
Li	210	208	184	176	165	159	153
Lu	0.35	0.27	0.25	0.37	0.17	0.13	0.33
Mn	394	390	856	527	272	51	564
Mo	3	2	<2	3	<2	<2	<2
Nb	26	32.7	13.2	24	12	8.7	16.6
Nd	46.9	11	41	29.8	6.3	19.8	26.7
Ni	22	<5	<5	10	<5	<5	10
Pb	21	30	20	24	22	8	23
Pr	13.21	3.54	11.1	8.96	2.56	5.39	7.53
Rb	178	160	194	210	197	442	136

Sample	RRSBH52-562	RRIO21-28	RRIO21-16	RRI022-64	RRIO21-20	RRMH21-6	RRMD21-4
Re	<0.02	<0.02	<0.02	<0.02	<0.02	<0.02	<0.02
Sb	4.6	0.9	1	0.9	2	8	2.1
Sc	8	<5	10	<5	<5	7	6
Se	<1	<5	<5	<1	<5	<5	<5
Sm	7.3	1.9	6.8	4.8	0.9	3.1	4.6
Sn	1	2	2	2	2	1	1
Sr	618	250	930	187	30.7	92	605
Ta	1	2.6	1	1.1	0.9	0.6	1.1
Tb	0.72	0.29	0.62	0.55	0.1	0.25	0.47
Te	<0.05	<0.5	<0.5	<0.05	<0.5	<0.5	<0.5
Th	16.4	24.9	8.4	15.7	17.5	11.8	16.5
Tl	0.5	0.9	<0.5	1.4	3.7	<0.5	0.9
Tm	0.34	0.23	0.26	0.34	0.09	0.11	0.28
U	6.68	4.33	1.76	5.6	4.92	9.03	4.15
V	96	<5	87	18	<5	63	48
W	2	2	3	1	1	5	3
Y	20	13.5	18.2	18.1	5	6.6	18.2
Yb	2.2	1.7	1.7	2.2	0.8	0.8	2.1
Zn	76	35	74	56	29	29	55
Zr	277	71.2	252	180	60.1	153	206

**Table 2.** New whole-rock geochemical data from the greater Rhyolite Ridge study area (continued).

Sample	RRIO22-54	RRIO21-10	RRIO21-36	RRIO21-35	RRIO21-14	RRIO21-4	RRIO21-1
Latitude	37.788857	37.819773	37.788665	37.784838	37.839276	37.815476	37.820112
Longitude	-117.877188	-117.828452	-117.896782	-117.897145	-117.868502	-117.868483	-117.855738
Map Unit	Tbi(?)	Ql (-Trt)	Trt	Trt	Tat	Trt	Trt
Lithology	basaltic intrusion	rhyolitic tuff block	rhyolitic tuff	volcanic breccia	rhyolitic tuff	fault breccia	rhyolitic tuff
<i>Major elements (wt %)</i>							
SiO <sub>2</sub>	51.4	62.7	57.59	71.93	72.07	64.74	68.17
TiO <sub>2</sub>	1.34	0.42	0.43	0.15	0.19	0.34	0.57
Al <sub>2</sub> O <sub>3</sub>	17.82	15.55	13.54	12.31	12.98	15.69	14.39
Fe <sub>2</sub> O <sub>3</sub>	8.23	2.58	2.53	0.99	1.23	2.13	3.03
MnO	0.08	0.05	0.08	0.04	0.06	0.25	0.04
MgO	1.93	0.85	1.05	0.4	0.44	0.96	0.69
CaO	5.56	2.42	3.53	0.72	1.35	2.13	1.8
Na <sub>2</sub> O	3.24	3.26	5.93	1.42	2.8	3.2	3
K <sub>2</sub> O	4.93	4.92	3.01	7.66	5.62	3.7	6.35
P <sub>2</sub> O <sub>5</sub>	0.64	0.08	0.13	0.02	0.02	0.08	0.18
SrO	--	0.03	0.08	0.05	0.03	0.06	0.05
BaO	0.16	0.1	0.12	0.01	0.06	0.11	0.15
V <sub>2</sub> O <sub>5</sub>	0.04	<0.01	<0.01	<0.01	<0.01	<0.01	<0.01
Cr <sub>2</sub> O <sub>3</sub>	0.01	<0.01	<0.01	<0.01	<0.01	<0.01	<0.01
LOI*	4.32957	6.86	11.52	3.88	3.02	6.71	1.43
Total	99.71	99.82	99.54	99.58	99.87	100.10	99.85
<i>Minor and trace elements (ppm)</i>							
Ag	<1	<1	<1	<1	<1	<1	<1
As	58	13	9	14	<5	10	516
B	92	50	80	451	42	61	283
Ba	1362	766	915	160	523	923	1210
Be	<5	<5	<5	<5	<5	<5	<5
Bi	<0.1	0.1	0.1	0.1	0.1	0.2	<0.1
Cd	<0.2	<0.2	<0.2	<0.2	<0.2	0.2	<0.2
Ce	100	133	76.6	70.5	66.4	75.7	103
Co	21.3	3.4	5.6	1.1	1.5	3.8	2.7
Cr	60	24	31	16	18	27	20
Cs	9.5	52.3	13.4	113	40.8	31.4	6.8
Cu	21	<5	7	<5	<5	<5	<5
Dy	5.05	3.54	3.03	2.18	1.89	2.93	2.58
Er	2.51	1.94	1.8	1.38	1.23	1.82	1.58
Eu	2.05	1.13	0.98	0.31	0.52	0.8	1.17
Ga	23	16.2	16.2	15.9	16.1	19.5	17.4
Gd	6.32	4.82	3.61	2.24	2.07	3.39	3.38
Ge	2	2	2	3	2	3	2
Hf	6	8	5	4	4	5	9
Ho	0.88	0.66	0.55	0.41	0.36	0.55	0.48
In	<0.2	<0.2	<0.2	<0.2	<0.2	<0.2	<0.2
La	49.7	73.2	41.1	42.6	40	39.8	57
Li	151	143	141	116	99	91	88
Lu	0.38	0.33	0.3	0.26	0.26	0.32	0.31
Mn	612	309	686	301	434	2340	250
Mo	<2	<2	<2	<2	<2	<2	13
Nb	17	17.6	14.4	18.9	13.7	22	21.3
Nd	45.8	43.1	27.2	18.5	19.1	24.9	31.4
Ni	46	<5	<5	<5	<5	<5	<5
Pb	12	27	23	29	20	56	20
Pr	11.8	12.4	7.53	6.12	6	7.21	9.52
Rb	157	186	131	243	221	171	167

<b>Sample</b>	<b>RRIO22-54</b>	<b>RRIO21-10</b>	<b>RRIO21-36</b>	<b>RRIO21-35</b>	<b>RRIO21-14</b>	<b>RRIO21-4</b>	<b>RRIO21-1</b>
<b>Re</b>	<0.02	<0.02	<0.02	<0.02	<0.02	<0.02	<0.02
<b>Sb</b>	0.6	1.3	2.8	1.7	0.6	5.4	16.5
<b>Sc</b>	17	<5	5	<5	<5	5	<5
<b>Se</b>	<1	<5	<5	<5	<5	<5	<5
<b>Sm</b>	7.6	6.4	4.6	3	2.8	4.5	4.6
<b>Sn</b>	2	2	1	1	2	1	1
<b>Sr</b>	867	312	654	461	273	451	494
<b>Ta</b>	0.8	1.2	1	1.4	0.9	1.8	1.2
<b>Tb</b>	0.89	0.61	0.48	0.33	0.3	0.48	0.45
<b>Te</b>	<0.05	<0.5	<0.5	<0.5	<0.5	<0.5	<0.5
<b>Th</b>	5	13.7	13.6	18.2	15.7	22.2	11.1
<b>Tl</b>	<0.5	<0.5	1.4	0.9	<0.5	11.8	<0.5
<b>Tm</b>	0.42	0.27	0.24	0.22	0.17	0.28	0.25
<b>U</b>	1.51	4.82	3.56	2.16	2.59	4.26	5.64
<b>V</b>	212	33	39	<5	13	33	44
<b>W</b>	2	<1	2	3	2	2	<1
<b>Y</b>	24.7	18.8	18.2	12.5	11.5	17.3	14.2
<b>Yb</b>	2.2	2	1.8	1.7	1.4	2.1	1.8
<b>Zn</b>	87	57	53	28	55	88	27
<b>Zr</b>	258	337	208	107	152	185	398

**Table 2.** New whole-rock geochemical data from the greater Rhyolite Ridge study area (continued).

Sample	MD22RR-1	MD22RR-1Dup	RRIO21-34	RRIO21-8	RRIO22-50	RRIO21-25	RRIO21-15
Latitude	37.7501	37.7501	37.781848	37.81978	37.822809	37.83984	37.778953
Longitude	-117.650598	-117.650598	-117.897398	-117.82558	-117.791503	-117.808474	-117.839509
Map Unit	KTg	KTg	Tai	Trt	Tbi	Tat	Trlb
Lithology	granite	granite	latite dike	reworked tuff	basaltic dike	rhyolitic tuff	rhyolite
<i>Major elements (wt %)</i>							
SiO <sub>2</sub>	71.61	71.72	80.52	60.97	50.16	61.14	73.34
TiO <sub>2</sub>	0.16	0.16	0.08	0.63	1.05	0.71	0.27
Al <sub>2</sub> O <sub>3</sub>	15.7	15.7	8.71	15.61	16.82	15.83	13.67
Fe <sub>2</sub> O <sub>3</sub>	1.34	1.34	0.61	3.59	8.43	3.28	1.89
MnO	0.04	0.04	0.04	0.06	0.13	0.08	0.05
MgO	0.26	0.26	0.15	1.36	5.7	1.09	0.29
CaO	2.11	2.09	1.3	3.82	8.92	2.78	1.22
Na <sub>2</sub> O	4.01	4.01	1.73	2.67	3.27	3.38	4.08
K <sub>2</sub> O	3.88	3.92	4.96	4.2	2.49	6.42	4.31
P <sub>2</sub> O <sub>5</sub>	0.07	0.07	0.02	0.24	0.56	0.17	0.04
SrO	--	--	0.02	0.19	--	0.06	<0.01
BaO	0.14	0.14	<0.01	0.19	0.18	0.21	0.11
V <sub>2</sub> O <sub>5</sub>	<0.01	<0.01	<0.01	0.01	0.03	<0.01	<0.01
Cr <sub>2</sub> O <sub>3</sub>	<0.01	<0.01	<0.01	<0.01	<0.01	<0.01	<0.01
LOI*	0.66993	0.85991	1.54	6.35	2.16978	4.63	0.73
Total	99.99	100.31	99.68	99.89	99.91	99.78	100.00
<i>Minor and trace elements (ppm)</i>							
Ag	<1	<1	<1	<1	<1	<1	<1
As	<5	<5	113	6	6	14	<5
B	<10	11	260	243	50	388	24
Ba	1190	1223	32.6	1560	1579	1800	863
Be	<5	<5	<5	<5	<5	<5	<5
Bi	<0.1	<0.1	<0.1	<0.1	<0.1	<0.1	0.3
Cd	<0.2	<0.2	<0.2	<0.2	<0.2	<0.2	<0.2
Ce	46.9	46.7	50.6	116	117	137	50.2
Co	1.1	0.9	<0.5	5.3	29.9	3.6	2
Cr	<10	<10	21	11	92	19	21
Cs	3.9	3.6	2.8	69.1	5.1	20.1	10.3
Cu	<10	<10	<5	<5	49	<5	6
Dy	1.77	1.75	1.95	3.55	4.66	4.71	3.8
Er	0.56	0.5	1.42	1.98	2.28	2.77	2.4
Eu	0.73	0.72	0.13	1.5	2.28	1.8	0.56
Ga	26	24	11.7	17.9	18	21.9	16.7
Gd	2.61	2.4	1.94	4.5	6.65	5.68	3.73
Ge	1	1	1	2	1	2	2
Hf	3	4	3	8	4	9	6
Ho	0.27	0.23	0.38	0.64	0.82	0.9	0.77
In	<0.2	<0.2	<0.2	<0.2	<0.2	<0.2	<0.2
La	27	26.5	29.3	63	55.5	71.5	25.8
Li	79	78	76	66	64	62	60
Lu	<0.05	0.08	0.27	0.31	0.36	0.43	0.36
Mn	279	284	287	485	1055	631	280
Mo	<2	<2	2	<2	<2	<2	2
Nb	23	23	17.9	19.2	11	23.4	8.1
Nd	18.3	17.2	13.3	40.3	54.1	49.1	18.8
Ni	<5	9	<5	<5	84	<5	<5
Pb	27	27	17	29	13	25	21
Pr	5.29	5.04	4.25	11.3	14.21	13.7	5
Rb	167	178	157	191	56.2	191	151

<b>Sample</b>	<b>MD22RR-1</b>	<b>MD22RR-1Dup</b>	<b>RRIO21-34</b>	<b>RRIO21-8</b>	<b>RRIO22-50</b>	<b>RRIO21-25</b>	<b>RRIO21-15</b>
<b>Re</b>	<0.02	<0.02	<0.02	<0.02	<0.02	<0.02	<0.02
<b>Sb</b>	<0.1	0.1	3.4	4	0.5	1.5	0.7
<b>Sc</b>	<5	<5	<5	6	23	7	<5
<b>Se</b>	<1	<1	<5	<5	<1	<5	<5
<b>Sm</b>	3.2	3	2.2	6.4	8.6	7.9	3.9
<b>Sn</b>	1	1	1	1	1	3	4
<b>Sr</b>	631	627	31.5	1690	1222	618	118
<b>Ta</b>	1.5	2	1.2	1.2	0.5	1.3	0.8
<b>Tb</b>	0.35	0.35	0.29	0.59	0.88	0.77	0.57
<b>Te</b>	<0.05	<0.05	<0.5	<0.5	<0.05	<0.5	<0.5
<b>Th</b>	5.7	6.2	15.4	10.8	6.2	12.4	15.1
<b>Tl</b>	1	0.9	<0.5	0.6	<0.5	<0.5	1
<b>Tm</b>	0.07	0.09	0.22	0.3	0.37	0.4	0.38
<b>U</b>	1.26	1.36	6.11	1.97	1.51	2.72	6.13
<b>V</b>	10	8	<5	65	189	47	12
<b>W</b>	<1	<1	2	<1	<1	5	1
<b>Y</b>	7.3	7.1	12.9	19.6	21.4	26.2	22.3
<b>Yb</b>	0.3	0.3	1.7	2	2.1	2.7	2.6
<b>Zn</b>	61	64	14	79	85	59	32
<b>Zr</b>	109	116	83.1	362	178	383	225

**Table 2.** New whole-rock geochemical data from the greater Rhyolite Ridge study area (continued).

Sample	RRIO21-18	RRIO21-27	RRIO21-30	RRIO21-23	MD22RR-128	RRIO21-19	MD22RR-97
Latitude	37.814654	37.826586	37.827692	37.795867	37.818863	37.821862	37.794097
Longitude	-117.783021	-117.845545	-117.892184	-117.803846	-117.790205	-117.786288	-117.8918
Map Unit	Zw	Tcsu	Tf	Trlb	Tat	Tbi	Tat
Lithology	phyllite	rhyolitic tuff	tuffaceous sandstone	rhyolite	rhyolitic tuff	basaltic dike	rhyolitic tuff
<b>Major elements (wt %)</b>							
SiO <sub>2</sub>	63.1	61.23	63.47	61.59	61.05	68.22	71.27
TiO <sub>2</sub>	0.68	0.71	0.7	0.7	0.8	0.59	0.33
Al <sub>2</sub> O <sub>3</sub>	16.2	15.9	15.78	16.3	17.18	14.7	15.06
Fe <sub>2</sub> O <sub>3</sub>	3.67	3.25	3.08	3.41	4.33	1.88	1.65
MnO	0.08	0.08	0.09	0.08	0.11	0.06	0.07
MgO	1.69	1.1	1.06	1	1.46	0.67	0.15
CaO	3.31	2.78	1.36	2.73	3.78	0.66	0.41
Na <sub>2</sub> O	3.88	3.33	1.29	2.77	4.16	2.22	4.17
K <sub>2</sub> O	4.58	6.46	10.06	7.13	4.86	9.41	6.89
P <sub>2</sub> O <sub>5</sub>	0.27	0.16	0.23	0.2	0.31	0.08	0.03
SrO	0.08	0.06	0.03	0.06	--	0.02	--
BaO	0.15	0.21	0.17	0.21	0.18	0.12	0.02
V <sub>2</sub> O <sub>5</sub>	0.01	<0.01	<0.01	<0.01	<0.01	<0.01	<0.01
Cr <sub>2</sub> O <sub>3</sub>	<0.01	<0.01	<0.01	<0.01	0.02	<0.01	<0.01
LOI*	2.35	4.61	2.52	3.52	2.09979	1.04	0.63006
Total	100.05	99.88	99.84	99.70	100.34	99.67	100.68
<b>Minor and trace elements (ppm)</b>							
Ag	<1	<1	<1	<1	<1	<1	<1
As	12	14	25	10	<5	127	13
B	18	394	642	355	73	275	27
Ba	1280	1710	1410	1920	1604	1010	254
Be	<5	<5	<5	<5	<5	<5	<5
Bi	<0.1	<0.1	<0.1	<0.1	<0.1	<0.1	<0.1
Cd	<0.2	<0.2	<0.2	<0.2	<0.2	<0.2	<0.2
Ce	126	130	120	129	118	74	155
Co	7.4	3.7	3.3	3	5.8	4.7	<0.5
Cr	30	25	18	15	<10	14	<10
Cs	8.5	19.6	12.9	21.8	2.2	3.5	2.2
Cu	13	<5	<5	<5	<10	<5	<10
Dy	4.13	4.63	3.95	4.3	4.38	2.04	5.48
Er	2.42	2.57	2.27	2.66	2.39	1.39	3.1
Eu	1.43	1.72	1.48	1.63	1.84	0.72	1
Ga	19.7	19.4	18.3	19.9	18	16.6	19
Gd	5.1	5.94	4.8	5.69	5.46	2.06	6.27
Ge	2	2	4	2	1	3	2
Hf	9	9	8	9	9	8	10
Ho	0.83	0.87	0.76	0.89	0.82	0.43	1.03
In	<0.2	<0.2	<0.2	<0.2	<0.2	<0.2	<0.2
La	66.8	67.8	62.9	68.5	62	43	80.4
Li	60	54	53	51	48	47	46
Lu	0.4	0.4	0.34	0.45	0.43	0.27	0.58
Mn	572	600	681	650	822	402	596
Mo	4	<2	<2	<2	<2	4	<2
Nb	22.5	22.9	19.7	22.8	22	19.6	36
Nd	42	46.6	41.9	45.6	45.6	21	56
Ni	<5	<5	5	<5	<5	<5	8
Pb	25	23	20	24	21	17	26
Pr	12.2	13	11.9	12.6	13.24	6.41	16.67
Rb	152	189	327	253	90.1	250	213

Sample	RRIO21-18	RRIO21-27	RRIO21-30	RRIO21-23	MD22RR-128	RRIO21-19	MD22RR-97
Re	<0.02	<0.02	<0.02	<0.02	<0.02	<0.02	<0.02
Sb	1.4	1.3	1.8	1.2	0.8	10	0.6
Sc	7	7	6	7	8	<5	<5
Se	<5	<5	<5	<5	<1	<5	<1
Sm	6.8	7.4	6.8	7	6.8	3.2	8.1
Sn	3	2	2	1	2	1	3
Sr	641	569	304	624	730	191	68
Ta	1.5	1.3	1.1	1.4	1.3	1.2	1.9
Tb	0.69	0.77	0.67	0.76	0.77	0.31	0.95
Te	<0.5	<0.5	<0.5	<0.5	<0.05	<0.5	<0.05
Th	15.4	11.6	11.1	11.5	11.2	10.6	19.6
Tl	0.7	<0.5	0.5	0.5	<0.5	<0.5	0.9
Tm	0.35	0.38	0.32	0.36	0.4	0.22	0.53
U	4.23	2.55	1.94	1.98	3.16	4.67	4.98
V	82	43	41	35	69	39	10
W	1	5	8	2	<1	1	2
Y	22.7	24.4	22.4	25.9	22.6	12	28.1
Yb	2.7	2.6	2.3	2.8	2.4	1.7	3.5
Zn	62	55	53	76	76	27	55
Zr	393	375	348	406	376	375	333

**Table 2.** New whole-rock geochemical data from the greater Rhyolite Ridge study area (continued).

Sample	RRIO21-6	RRIO21-40	RRIO21-40Dup	RRMD21-1	RRIO21-9	RRIO21-9Dup	RRSBHC10-630
Latitude	37.820039	37.803105	37.803105	37.807574	37.81979	37.81979	37.805645
Longitude	-117.871815	-117.89552	-117.89552	-117.790912	-117.82583	-117.82583	-117.848397
Map Unit	Ts	Tf	Tf	Trlb	Tat?	Tat?	Trt
Lithology	pebbly sandstone	reworked tuff	reworked tuff	rhyolite	rhyolitic tuff	rhyolitic tuff	rhyolitic tuff
<b>Major elements (wt %)</b>							
SiO <sub>2</sub>	60.2	72.39	54.61	72.62	77.86	70.79	68.65
TiO <sub>2</sub>	0.68	0.13	0.63	0.1	0.1	0.12	0.14
Al <sub>2</sub> O <sub>3</sub>	15.99	12.15	22.49	12.32	11.51	11.93	13.12
Fe <sub>2</sub> O <sub>3</sub>	3.8	0.72	3.13	0.75	0.72	0.77	0.78
MnO	0.05	0.02	0.07	0.09	0.04	0.05	0.02
MgO	1.51	0.19	1.3	0.36	0.17	0.21	0.43
CaO	4.57	0.56	3.87	0.39	0.84	1.61	1.28
Na <sub>2</sub> O	2.59	2.7	1.9	2.9	3.34	2.69	1.45
K <sub>2</sub> O	3.6	5.67	4.64	5.72	4.5	3.88	8.22
P <sub>2</sub> O <sub>5</sub>	0.17	0.01	0.2	<0.01	0.02	0.02	0.02
SrO	0.06	0.03	0.05	<0.01	<0.01	0.02	0.02
BaO	0.2	0.02	0.16	<0.01	0.01	0.01	<0.01
V <sub>2</sub> O <sub>5</sub>	0.02	<0.01	0.01	<0.01	<0.01	<0.01	<0.01
Cr <sub>2</sub> O <sub>3</sub>	0.01	<0.01	<0.01	<0.01	<0.01	<0.01	<0.01
LOI*	6.69	5.13	6.98	4.39	0.73	7.73	5.67
Total	100.14	99.72	100.04	99.64	99.84	99.83	99.80
<b>Minor and trace elements (ppm)</b>							
Ag	<1	<1	<1	<1	<1	<1	<1
As	22	14	9	10	8	<5	10
B	20	23	90	83	30	40	31
Ba	1680	91.8	1320	13.2	105	97.1	60.6
Be	<5	<5	<5	7	<5	<5	<5
Bi	0.1	0.1	<0.1	0.4	0.1	0.2	0.1
Cd	<0.2	<0.2	0.3	<0.2	<0.2	<0.2	<0.2
Ce	78.6	66.1	110	51.7	45	44.7	99.7
Co	13	<0.5	5.4	<0.5	0.9	0.6	0.5
Cr	62	11	25	11	13	14	13
Cs	13.8	20.1	33.1	9.7	4.5	41.3	20.3
Cu	17	<5	<5	<5	<5	<5	<5
Dy	2.98	2.39	3.99	4.77	0.77	0.75	3.38
Er	1.64	1.51	2.34	2.77	0.74	0.71	2.19
Eu	1.34	0.21	1.34	0.08	0.15	0.16	0.34
Ga	19.5	16.1	20.9	19.5	15.7	15.8	18.9
Gd	3.85	2.37	4.93	4.53	0.78	0.76	3.63
Ge	2	2	2	3	2	1	2
Hf	5	4	7	5	3	3	5
Ho	0.55	0.47	0.73	0.9	0.19	0.17	0.67
In	<0.2	<0.2	<0.2	<0.2	<0.2	<0.2	<0.2
La	44.2	38.7	58.3	21.2	32.3	32.7	57.5
Li	45	43	112	43	42	21	41
Lu	0.24	0.26	0.39	0.42	0.22	0.19	0.4
Mn	451	85	502	697	244	303	118
Mo	<2	<2	<2	5	<2	3	<2
Nb	10.3	24	18.2	41.9	16.5	14.3	26.9
Nd	30.6	17.9	40.1	19.2	7.9	8.1	28.7
Ni	10	<5	<5	<5	<5	<5	<5
Pb	24	45	20	42	26	25	18
Pr	8.33	5.78	10.8	5.56	3.13	3.14	8.97
Rb	120	224	178	243	181	204	268

Sample	RRIO21-6	RRIO21-40	RRIO21-40Dup	RRMD21-1	RRIO21-9	RRIO21-9Dup	RRSBHC10-630
<b>Re</b>	<0.02	<0.02	<0.02	<0.02	<0.02	<0.02	<0.02
<b>Sb</b>	3.2	0.7	1.4	1.7	1.1	0.5	5.3
<b>Sc</b>	13	<5	7	<5	<5	<5	<5
<b>Se</b>	<5	<5	<5	<5	<5	<5	<5
<b>Sm</b>	5.1	3	6.6	4.4	1.1	1	4.9
<b>Sn</b>	1	2	2	2	2	2	2
<b>Sr</b>	677	205	489	17.5	55.9	188	205
<b>Ta</b>	0.7	1.5	1.1	3.4	1	1	1.7
<b>Tb</b>	0.51	0.36	0.68	0.75	0.11	0.12	0.53
<b>Te</b>	<0.5	<0.5	<0.5	<0.5	<0.5	<0.5	<0.5
<b>Th</b>	16.3	18.1	10.1	24.8	22.1	20.8	21.6
<b>Tl</b>	0.8	<0.5	0.7	1.6	0.8	0.7	5.2
<b>Tm</b>	0.22	0.22	0.36	0.42	0.14	0.12	0.35
<b>U</b>	5.17	5.26	2.16	11.2	6.65	4.56	6.25
<b>V</b>	103	<5	56	<5	<5	6	<5
<b>W</b>	1	2	1	3	2	1	2
<b>Y</b>	15.4	14.1	22.2	28.3	7	6.5	21.8
<b>Yb</b>	1.6	1.8	2.3	3.2	1.2	1.1	2.5
<b>Zn</b>	53	17	61	61	20	23	34
<b>Zr</b>	202	121	320	93	72.7	89	121

**Table 2.** New whole-rock geochemical data from the greater Rhyolite Ridge study area (continued).

Sample	RRIO22-65	RRIO21-2	RRIO21-2Dup	RRIO22-51	RRIO22-51Dup	RRIO21-7	RRIO22-63
Latitude	37.641465	37.808043	37.808043	37.840268	37.840268	37.821058	37.864152
Longitude	-117.496321	-117.835944	-117.835944	-117.874437	-117.874437	-117.869371	-117.827201
Map Unit	Trt	Trt	Trt	Trt	Trt	Trt	Tic
Lithology	rhyolitic tuff	tuff breccia	tuff breccia	rhyolitic tuff	rhyolitic tuff	rhyolitic tuff	rhyolitic tuff
<i>Major elements (wt %)</i>							
SiO <sub>2</sub>	67.89	77.22	77.02	70.33	69.9	62.45	66.47
TiO <sub>2</sub>	0.21	0.14	0.12	0.12	0.12	0.85	0.23
Al <sub>2</sub> O <sub>3</sub>	12.57	12.36	10.94	11.68	11.56	17	13.82
Fe <sub>2</sub> O <sub>3</sub>	1.12	0.77	0.68	0.9	0.9	4.76	1.91
MnO	0.04	0.03	0.01	0.04	0.05	0.04	0.01
MgO	0.48	0.1	0.08	0.19	0.18	0.67	0.93
CaO	2.24	0.38	0.54	1.37	1.37	3.27	1.69
Na <sub>2</sub> O	1.61	3.54	0.78	2.21	2.2	4.29	2.27
K <sub>2</sub> O	4.82	5.34	8.53	4.52	4.48	5.3	4.35
P <sub>2</sub> O <sub>5</sub>	0.04	0.01	0.03	0.01	0.01	0.46	0.05
SrO	--	<0.01	<0.01	--	--	0.07	--
BaO	0.03	0.01	0.03	<0.01	0.01	0.17	0.12
V <sub>2</sub> O <sub>5</sub>	<0.01	<0.01	<0.01	<0.01	<0.01	0.01	<0.01
Cr <sub>2</sub> O <sub>3</sub>	<0.01	<0.01	<0.01	<0.01	<0.01	<0.01	<0.01
LOI*	9.34	0.35	1	9.05091	9.32093	0.74	8.46
Total	100.39	100.25	99.76	100.42	100.10	100.08	100.31
<i>Minor and trace elements (ppm)</i>							
Ag	<1	<1	<1	<1	<1	<1	<1
As	<5	17	41	11	11	<5	9
B	37	45	784	86	81	31	28
Ba	247	65.5	246	89	87	1340	1029
Be	<5	<5	<5	<5	<5	<5	<5
Bi	0.2	<0.1	0.1	<0.1	<0.1	<0.1	<0.1
Cd	<0.2	<0.2	<0.2	<0.2	<0.2	<0.2	<0.2
Ce	80.9	75.4	56.1	69.8	64.6	133	78
Co	1.7	<0.5	0.6	<0.5	<0.5	7.7	1.7
Cr	<10	17	14	10	<10	25	<10
Cs	13.7	5.7	2.1	32.7	32.9	61.6	17.9
Cu	<10	<5	<5	<10	<10	<5	<10
Dy	3.06	2.74	1.06	2.82	2.65	4.27	2.92
Er	1.99	1.89	0.66	1.82	1.61	2.31	1.47
Eu	0.5	0.23	0.24	0.27	0.25	1.59	0.8
Ga	17	16	13.9	15	14	18.5	16
Gd	3.24	2.78	1.28	2.63	2.62	5.18	3.66
Ge	<1	2	1	<1	<1	5	2
Hf	5	4	3	4	4	9	5
Ho	0.64	0.56	0.23	0.55	0.48	0.77	0.5
In	<0.2	<0.2	<0.2	<0.2	<0.2	<0.2	<0.2
La	46	43.5	36	39.8	38	69.8	40.8
Li	40	34	83	34	39	33	33
Lu	0.37	0.35	0.13	0.35	0.36	0.35	0.27
Mn	276	136	42	328	326	258	134
Mo	<2	<2	7	<2	<2	<2	<2
Nb	24	23.3	18.5	26	26	23.1	17
Nd	28.6	21.1	12.3	20.2	19.2	45.7	28.6
Ni	9	<5	<5	12	12	<5	7
Pb	24	29	24	24	24	20	24
Pr	8.77	6.64	4.25	6.74	6.48	13.2	8.41
Rb	164	170	193	243	238	257	155

Sample	RRIO22-65	RRIO21-2	RRIO21-2Dup	RRIO22-51	RRIO22-51Dup	RRIO21-7	RRIO22-63
Re	<0.02	<0.02	<0.02	<0.02	<0.02	<0.02	<0.02
Sb	1	3.9	2	0.8	1	0.9	1.1
Sc	<5	<5	<5	<5	<5	9	<5
Se	<1	<5	<5	<1	<1	<5	<1
Sm	4.6	3.5	1.8	3.3	3.3	7	4.7
Sn	2	1	<1	2	2	1	2
Sr	221	26.3	75.7	698	699	693	1064
Ta	1.2	1.6	1	1.6	1.6	1.4	1.1
Tb	0.5	0.42	0.21	0.46	0.44	0.71	0.54
Te	<0.05	<0.5	<0.5	<0.05	<0.05	<0.5	<0.05
Th	16.8	18.5	16.1	19.4	18.2	12.7	22.7
Tl	1.1	0.6	0.7	0.9	0.9	<0.5	0.8
Tm	0.33	0.32	0.11	0.32	0.31	0.33	0.26
U	5.44	5.14	3.44	3.15	2.91	3.6	2.8
V	16	<5	<5	<5	<5	89	14
W	<1	6	3	1	1	2	2
Y	17.7	18.8	6.8	14.9	14.7	21.7	13.5
Yb	2.2	2.3	0.8	2	2	2.5	1.4
Zn	33	15	35	33	36	65	47
Zr	162	111	143	103	106	384	161

**Table 2.** New whole-rock geochemical data from the greater Rhyolite Ridge study area (continued).

Sample	RRIO22-45	RRIO22-59	RRIO22-60B	RRIO21-13	RRIO22-58A	RRSBH88-229	RRMH21-3
Latitude	37.840901	37.912321	37.942399	37.839453	37.816897	37.800272	37.797726
Longitude	-117.818812	-117.991854	-118.076274	-117.86704	-117.918254	-117.858434	-117.81933
Map Unit	Tbi	Trt	Trt	Trt	Trlb	Tal	Trlb
Lithology	basaltic intrusion	rhyolitic tuff	rhyolitic tuff	rhyolitic tuff	rhyolitic tuff (fresh)	latite	perlitic rhyolite
<i>Major elements (wt %)</i>							
SiO <sub>2</sub>	48.15	68.78	73.41	50.22	75.13	67.83	64.18
TiO <sub>2</sub>	1.08	0.14	0.12	1.05	0.09	0.68	0.81
Al <sub>2</sub> O <sub>3</sub>	21.21	11.72	12.26	17.05	10.92	14.49	16.83
Fe <sub>2</sub> O <sub>3</sub>	7.66	0.86	0.85	8.74	0.53	4.18	3.72
MnO	0.11	0.02	0.06	0.14	0.01	0.04	0.06
MgO	4.51	0.15	0.2	6.05	0.53	1.04	0.7
CaO	10.85	0.4	0.53	9.46	0.45	2.1	0.92
Na <sub>2</sub> O	2.56	4.02	3.25	3.2	1.25	2.53	2.58
K <sub>2</sub> O	1.92	4.33	5.51	2.32	6.13	5.14	7.92
P <sub>2</sub> O <sub>5</sub>	0.55	0.02	0.02	0.55	0.01	0.27	0.32
SrO	--	--	--	0.15	--	0.02	0.03
BaO	0.15	<0.01	<0.01	0.19	<0.01	0.16	0.2
V <sub>2</sub> O <sub>5</sub>	0.03	<0.01	<0.01	0.04	<0.01	0.01	0.01
Cr <sub>2</sub> O <sub>3</sub>	<0.01	<0.01	<0.01	0.02	<0.01	<0.01	<0.01
LOI*	1.21	9.82	4.73047	1.5	5.44946	1.16	1.6
Total	99.99	100.26	100.94	100.68	100.50	99.65	99.88
<i>Minor and trace elements (ppm)</i>							
Ag	<1	<1	<1	<1	<1	3	<1
As	<5	9	<5	<5	<5	33	<5
B	35	47	76	<10	37	<10	<10
Ba	1139	68	98	1460	27	1290	1740
Be	<5	<5	<5	<5	<5	<5	<5
Bi	<0.1	<0.1	<0.1	<0.1	<0.1	4.5	<0.1
Cd	<0.2	<0.2	<0.2	<0.2	<0.2	0.3	<0.2
Ce	65.7	64.5	73.2	119	36.8	441	142
Co	26	<0.5	<0.5	31.7	<0.5	6.5	3.3
Cr	29	<10	11	106	<10	24	13
Cs	1.3	33.9	5.7	2.7	28.4	2	5.4
Cu	43	<10	<10	46	<10	34	<5
Dy	3.18	2.55	2.8	4.2	0.68	5.76	4.53
Er	1.69	1.5	1.85	2.29	0.6	2.49	2.73
Eu	1.63	0.32	0.26	2.17	0.17	2.16	1.79
Ga	20	15	15	18.2	13	22.3	19.7
Gd	4.55	2.56	2.86	6.12	0.75	12.7	5.88
Ge	1	<1	1	2	2	2	2
Hf	4	5	5	4	3	15	9
Ho	0.63	0.47	0.56	0.8	0.14	0.97	0.86
In	<0.2	<0.2	<0.2	<0.2	<0.2	<0.2	<0.2
La	32.4	38.2	41.7	57.4	28.9	193	73.3
Li	32	31	31	30	30	29	28
Lu	0.23	0.32	0.4	0.35	0.26	0.24	0.47
Mn	815	185	456	1110	104	283	423
Mo	<2	<2	3	<2	<2	<2	2
Nb	9	26	26	9.9	18	23.4	24.5
Nd	34.2	19.7	21.2	51.6	7.8	196	49.3
Ni	32	8	10	75	11	<5	<5
Pb	6	17	28	14	13	38	20
Pr	8.49	6.57	7.05	13.3	3.08	51.6	14.2
Rb	32.1	211	189	48.5	181	231	243

Sample	RRIO22-45	RRIO22-59	RRIO22-60B	RRIO21-13	RRIO22-58A	RRSBH88-229	RRMH21-3
Re	<0.02	<0.02	<0.02	<0.02	<0.02	<0.02	<0.02
Sb	<0.1	2	0.6	0.1	4.3	0.8	5.2
Sc	17	<5	<5	23	<5	6	7
Se	<1	<1	<1	<5	<1	<5	<5
Sm	5.9	3.1	3.3	8.6	0.8	25.4	8.3
Sn	2	2	2	1	1	5	1
Sr	1334	231	53	1300	76	232	231
Ta	<0.5	1.6	1.8	0.6	1	8.1	1.4
Tb	0.6	0.44	0.48	0.76	0.14	1.23	0.77
Te	<0.05	<0.05	0.07	<0.5	<0.05	4.3	<0.5
Th	5.3	19	20.2	6.2	19.9	112	13
Tl	<0.5	0.5	1	<0.5	1.2	2.2	1.5
Tm	0.24	0.3	0.35	0.29	0.16	0.28	0.39
U	0.66	5.11	5.67	1.53	4.09	2.85	3.48
V	175	7	<5	193	<5	74	62
W	<1	1	1	<1	<1	7	3
Y	15	14.1	16.7	20.9	5.5	25.8	25.6
Yb	1.5	1.7	2.3	2.1	1.1	1.7	2.9
Zn	70	32	39	76	41	115	69
Zr	144	138	128	181	63	664	420

**Table 2.** New whole-rock geochemical data from the greater Rhyolite Ridge study area (continued).

Sample	RRIO21-33	RRIO21-32	RRIO22-57	RRIO21-26	MD22RR-3	RRIO22-41	RRMH21-2
Latitude	37.777172	37.833851	37.811228	37.839074	37.78436	37.858785	37.797149
Longitude	-117.902973	-117.905598	-117.911555	-117.80918	-117.72691	-117.827872	-117.818714
Map Unit	Tai	Tf	Ts	Trt	KTg	Trt	Trt
Lithology	latite dike	tuffaceous sandstone	rhyolitic tuff	rhyolitic tuff	granite	rhyolitic tuff	rhyolitic tuff
<b>Major elements (wt %)</b>							
SiO <sub>2</sub>	73.41	74.82	76.81	67.39	72.25	62.69	64.49
TiO <sub>2</sub>	0.24	0.19	0.22	0.28	0.11	0.39	0.77
Al <sub>2</sub> O <sub>3</sub>	12.78	12.98	11.39	13.62	14.95	16.41	16.41
Fe <sub>2</sub> O <sub>3</sub>	0.36	0.64	1.08	1.34	1.1	1.47	3.92
MnO	0.02	0.02	0.06	0.04	0.02	<0.01	0.08
MgO	0.14	0.1	0.11	0.28	0.21	0.26	0.93
CaO	0.9	0.53	0.53	0.69	1.03	2.29	2.48
Na <sub>2</sub> O	2.41	1.88	3.47	3.4	3.13	1.52	4.15
K <sub>2</sub> O	7.04	7.91	4.75	5.88	6.21	11.04	5.58
P <sub>2</sub> O <sub>5</sub>	0.02	0.02	0.03	0.02	0.06	0.12	0.32
SrO	0.01	0.02	--	0.02	--	--	0.05
BaO	0.05	0.04	0.01	0.03	0.14	0.07	0.15
V <sub>2</sub> O <sub>5</sub>	<0.01	<0.01	<0.01	<0.01	<0.01	<0.01	0.02
Cr <sub>2</sub> O <sub>3</sub>	<0.01	<0.01	<0.01	<0.01	<0.01	<0.01	<0.01
LOI*	2.15	0.85	1.73965	6.89	0.88	4.44956	0.55
Total	99.53	100.00	100.20	99.88	100.09	100.71	99.90
<b>Minor and trace elements (ppm)</b>							
Ag	<1	<1	<1	<1	<1	<1	<1
As	16	23	<5	9	<5	135	8
B	817	346	43	53	18	75	<10
Ba	464	300	88	281	1317	610	1180
Be	<5	<5	<5	<5	<5	<5	<5
Bi	0.1	0.1	<0.1	0.1	<0.1	0.2	<0.1
Cd	<0.2	<0.2	<0.2	<0.2	<0.2	<0.2	<0.2
Ce	75.8	57.2	123	120	18.8	161	146
Co	<0.5	0.6	<0.5	2.3	1	0.6	7.5
Cr	26	15	<10	15	<10	<10	25
Cs	8.3	4.7	4.9	59.3	2.6	2.1	2.7
Cu	<5	<5	<10	<5	<10	<10	9
Dy	2.1	1.17	5.27	3.69	1.03	4.26	4.41
Er	1.04	0.7	2.79	2.24	0.5	2.08	2.78
Eu	0.66	0.37	0.92	0.65	0.5	1.09	1.48
Ga	16.3	15.5	14	16	21	19	19.4
Gd	2.65	1.36	5.7	4.52	1.42	5.59	5.87
Ge	1	2	1	1	1	7	3
Hf	5	4	8	6	3	8	10
Ho	0.36	0.21	0.93	0.72	0.2	0.75	0.88
In	<0.2	<0.2	<0.2	<0.2	<0.2	<0.2	<0.2
La	41.4	37.2	62.1	66.2	11	87	77.2
Li	27	25	25	24	22	22	22
Lu	0.19	0.14	0.47	0.37	0.08	0.38	0.46
Mn	42	47	456	280	246	27	672
Mo	2	<2	<2	<2	<2	10	<2
Nb	25.5	13.2	27	21.3	14	25	26
Nd	24.1	13.3	47.4	37.1	7.7	56.1	50.3
Ni	<5	<5	10	<5	15	9	<5
Pb	18	18	21	23	36	28	24
Pr	7.08	4.49	13.75	11.3	2.15	17.24	14.3
Rb	164	201	128	261	209	339	149

Sample	RRIO21-33	RRIO21-32	RRIO22-57	RRIO21-26	MD22RR-3	RRIO22-41	RRMH21-2
Re	<0.02	<0.02	<0.02	<0.02	<0.02	<0.02	<0.02
Sb	1.7	1.5	0.4	3	<0.1	7.3	0.4
Sc	<5	<5	<5	<5	<5	<5	7
Se	<5	<5	<1	<5	<1	<1	<5
Sm	4.2	2	7.7	5.9	1.6	8.3	7.8
Sn	1	1	2	2	2	3	1
Sr	174	138	60	239	452	211	483
Ta	1.4	0.9	1.4	1.4	<0.5	1.5	1.6
Tb	0.35	0.18	0.91	0.62	0.21	0.78	0.74
Te	<0.5	<0.5	<0.05	<0.5	<0.05	<0.05	<0.5
Th	15.4	15.4	12.5	17.1	4.1	17.8	15.5
Tl	0.5	1	<0.5	0.6	1.2	2.6	0.8
Tm	0.16	0.11	0.45	0.33	0.08	0.37	0.4
U	9.56	3.78	3.09	3.62	1.32	10.68	5.14
V	11	10	5	13	8	26	75
W	4	4	3	2	<1	13	2
Y	9.9	6.7	25.2	20.4	4.8	19	25.3
Yb	1.3	1	2.9	2.3	0.5	2.2	2.9
Zn	<5	5	33	45	41	10	85
Zr	214	120	277	222	78	268	437

**Table 2.** New whole-rock geochemical data from the greater Rhyolite Ridge study area (continued)

Sample	RRMH21-4	RRIO21-17	MD22RR-2	RRIO22-58B	RRIO21-11	RRIO22-47	RRIO21-31
Latitude	37.808357	37.778242	37.770766	37.816897	37.837394	37.789123	37.83392
Longitude	-117.838872	-117.84589	-117.704915	-117.918254	-117.863943	-117.887525	-117.905712
Map Unit	Tat	Trt	KTg	Trlb	Trt	Ts	QTf
Lithology	rhyolitic tuff	rhyolitic tuff	granite	rhyolitic tuff (altered)	rhyolitic tuff	baked sandstone	rhyolitic tuff
<b>Major elements (wt %)</b>							
SiO <sub>2</sub>	59.47	67.42	71.43	71.53	69.33	63.48	67.07
TiO <sub>2</sub>	0.55	0.43	0.14	0.11	0.4	0.81	0.65
Al <sub>2</sub> O <sub>3</sub>	14.15	14.3	15.21	11.76	15.55	16.64	15.78
Fe <sub>2</sub> O <sub>3</sub>	2.83	2.61	1.35	0.72	2.62	3.88	3.06
MnO	0.08	0.06	0.02	0.07	0.06	0.08	0.04
MgO	0.71	0.89	0.3	0.42	0.74	0.77	0.54
CaO	5.69	2.62	1.71	0.68	1.94	2.72	1.86
Na <sub>2</sub> O	2.44	3.28	3.08	2.99	3.88	4.52	4.07
K <sub>2</sub> O	8.12	4.19	5.25	3.32	4.12	5.02	5.22
P <sub>2</sub> O <sub>5</sub>	0.21	0.18	0.08	0.02	0.22	0.34	0.15
SrO	0.03	0.09	--	--	0.07	--	0.08
BaO	0.14	0.14	0.21	0.02	0.25	0.2	0.17
V <sub>2</sub> O <sub>5</sub>	<0.01	<0.01	<0.01	<0.01	<0.01	0.01	<0.01
Cr <sub>2</sub> O <sub>3</sub>	<0.01	<0.01	<0.01	<0.01	<0.01	<0.01	<0.01
LOI*	4.62	3.81	1.19012	8.57	0.76	1.44014	1.21
Total	99.04	100.02	99.97	100.21	99.94	99.91	99.90
<b>Minor and trace elements (ppm)</b>							
Ag	<1	<1	3	<1	<1	<1	<1
As	132	<5	<5	<5	<5	6	45
B	252	<10	<10	56	<10	27	73
Ba	1120	1210	1824	188	2000	1653	1420
Be	<5	<5	<5	<5	9	<5	<5
Bi	<0.1	0.1	<0.1	<0.1	<0.1	<0.1	<0.1
Cd	<0.2	<0.2	<0.2	<0.2	<0.2	<0.2	<0.2
Ce	110	85.8	47.9	41	106	121	113
Co	4.5	3.5	0.9	<0.5	3.7	4.2	3.3
Cr	18	19	<10	<10	16	<10	18
Cs	1.9	1.6	2.7	116	4.2	2.2	2.2
Cu	<5	<5	<10	<10	<5	<10	<5
Dy	3.47	3.45	1.38	0.78	1.72	4.57	3.26
Er	2.11	2.13	0.41	0.64	0.96	2.73	2.16
Eu	1.28	0.84	0.66	0.19	0.87	1.79	1.21
Ga	16.7	17.3	20	15	20.9	20	18.4
Gd	4.11	3.86	2.46	0.87	2.72	5.68	3.85
Ge	2	2	1	1	2	1	2
Hf	8	6	3	3	4	9	9
Ho	0.66	0.69	0.2	0.14	0.3	0.91	0.6
In	<0.2	<0.2	<0.2	<0.2	<0.2	<0.2	<0.2
La	59.9	46.2	26.7	29.3	60.4	63.6	61.1
Li	21	20	19	19	18	16	11
Lu	0.33	0.35	<0.05	0.25	0.13	0.44	0.41
Mn	612	548	148	501	436	552	307
Mo	4	<2	<2	<2	<2	3	4
Nb	19.7	17	9	17	17.5	26	21.9
Nd	37.7	29.8	18.9	8.1	32.1	50.5	34.5
Ni	<5	<5	5	9	<5	9	<5
Pb	19	20	26	33	26	22	20
Pr	10.7	8.42	5.43	3.27	9.49	14.12	10.3
Rb	213	96.8	165	378	140	110	97.6

Sample	RRMH21-4	RRIO21-17	MD22RR-2	RRIO22-58B	RRIO21-11	RRIO22-47	RRIO21-31
Re	<0.02	<0.02	<0.02	<0.02	<0.02	<0.02	<0.02
Sb	3.9	0.6	<0.1	1.8	<0.1	0.9	1
Sc	<5	<5	<5	<5	<5	6	<5
Se	<5	<5	<1	<1	<5	<1	<5
Sm	5.5	4.9	3.4	1	4	7.8	5.2
Sn	2	1	2	2	3	1	2
Sr	283	943	700	212	688	597	664
Ta	1.3	1.1	<0.5	1.1	4.2	0.8	1.3
Tb	0.56	0.58	0.32	0.15	0.33	0.8	0.55
Te	<0.5	<0.5	<0.05	<0.05	<0.5	<0.05	<0.5
Th	12.2	12.8	8.4	21.1	13.1	11.8	12.7
Tl	<0.5	0.6	1	3.2	0.7	0.6	1.1
Tm	0.31	0.32	<0.05	0.17	0.13	0.4	0.32
U	4.3	5.41	1.13	5.67	2.1	2.88	6.91
V	44	32	7	6	39	66	47
W	<1	<1	<1	1	<1	2	6
Y	20.1	19.9	4.9	5.9	9.9	23.6	17.4
Yb	2.2	2.3	0.3	1.1	0.9	2.8	2.5
Zn	40	60	48	40	66	68	31
Zr	360	218	120	72.1	187	362	389

Abbreviations: "Dup" in sample name indicates a duplicate analysis.

\*LOI—loss on ignition.

All analyses performed by AGAT Laboratories via inductively coupled plasma-optical emission spectrometry (ICP-OES) and inductively coupled plasma-mass spectrometry (ICP-MS) methods for minor and trace elements, and Wavelength Dispersive X-ray Fluorescence (WDXR) for major element oxides.

Sample names in italic are not shown on map.